Gradient scaffolds for osteochondral tissue engineering and regeneration

Bin Zhang [a], Jie Huang *[a] and Roger J. Narayan *[b]

[a] Department of Mechanical Engineering, University College London, London, UK.

*Corresponding author. E-mail: jie.huang@ucl.ac.uk

[b] Joint Department of Biomedical Engineering, University of North Carolina and North Carolina State University, Raleigh, North Carolina, USA.

*Corresponding author. E-mail: roger_narayan@unc.edu

Abstract

The tissue engineering approach for repairing osteochondral (OC) defects involves the fabrication of a biological tissue scaffold that mimics the physiological properties of natural OC tissue (e.g., the gradient transition between the cartilage surface and the subchondral bone). The OC tissue scaffolds described in many research studies exhibit a discrete gradient (e.g., a biphasic or tri/multiphasic structure) or continuous gradient to mimic OC tissue attributes such as biochemical composition, structure, and mechanical properties. One advantage of a continuous gradient scaffold over biphasic or tri/multiphasic tissue scaffolds is that more closely mimics natural OC tissue since there is no distinct interface between each layer. Although research studies to this point have yielded good results related to OC regeneration with tissue scaffolds, differences between engineered scaffolds and natural OC tissue remain; due to these differences, current clinical therapies to repair OC defects with engineered scaffolds have not been successful.

This paper provides an overview of both discrete and continuous gradient OC tissue scaffolds in terms of cell type, scaffold material, microscale structure, mechanical properties, fabrication methods, and scaffold stimuli. Fabrication of gradient scaffolds with three-dimensional (3D) printing is given special emphasis due to its ability to accurately control scaffold pore geometry. Moreover, the application of computational modeling in OC tissue engineering is considered; for example, efforts to optimize scaffold structure, mechanical properties, and physical stimuli generated within the scaffold-bioreactor system to predict tissue regeneration are considered. Finally, challenges associated with the repair of OC defects and recommendations for future directions in OC tissue regeneration are proposed.

Keywords: osteochondral tissue, gradient scaffold, 3D printing, computational modeling.

Statement of significance

The submitted review paper entitled “Gradient scaffolds for osteochondral tissue engineering and regeneration” is a review that considers the application of tissue engineering for repairing osteochondral tissue. The use of discrete and continuous gradient scaffolds to mimic the transition properties between the articular cartilage and subchondral bone has been reviewed in this paper. Moreover, we also give an overview of recent studies involving the application of 3D printing techniques for osteochondral tissue scaffold production and the application of computational modeling for the prediction of osteochondral tissue regeneration in scaffold-bioreactor systems. This summarised information may be a useful resource for biomedical researchers.

Graphical abstract

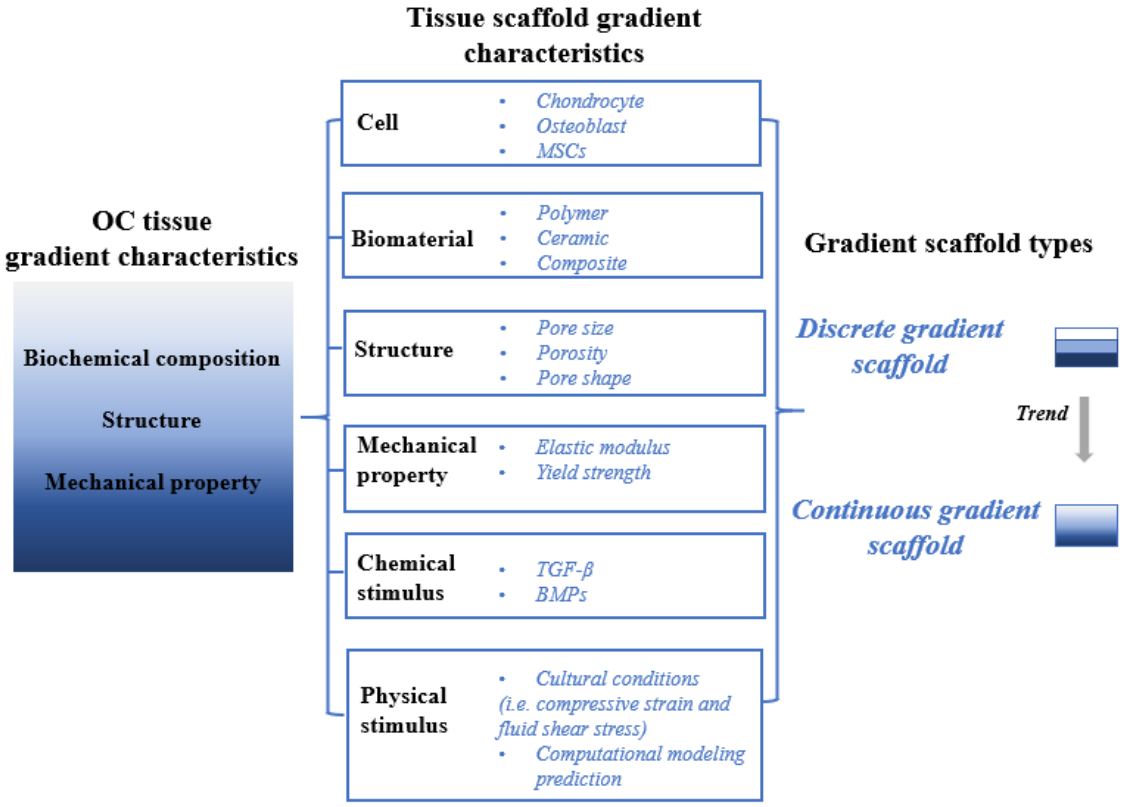

1 Introduction

Osteochondral defects can lead to joint malfunction and the development of degenerative diseases such as osteoarthritis. It has been estimated by the World Health Organization that 9.6% of men and 18.0% of women over the age of sixty suffer from symptomatic osteoarthritis. Among them, there are 80% have limitations in mobility, and 25% are unable to perform major daily activities [1]. OC defects have a limited capacity for spontaneous healing due to the poor healing capabilities of cartilage; these defects can lead to catastrophic degenerative arthritis [2]. Clinical findings have indicated that there is no existing medication substantially promotes the healing process; as such, surgical replacement is required for OC tissue repair. The current surgical treatments for OC defects depends on lesion severity; for instance, intra-articular injections of mesenchymal stem cells with platelet-rich plasma and bone marrow stimulation are used for early-stage lesions; autograft, allograft, or total joint replacement is required for severe degeneration [3-5]. Among surgical treatments, repair using autograft or allograft is limited due to the insufficient supply of autograft material and potential risk of viral transmission with allograft material [6,7].

Tissue engineering is regarded as a promising approach for OC tissue regeneration, which overcomes the limitations associated with the use of allograft and autograft tissue [8-17]. Considering that the OC defect often involves damage to both the cartilage and the underlying subchondral bone, tissue scaffolds must have a discrete gradient or a continuous gradient in terms of cell composition, growth factor, material composition, structure, mechanical properties, and cell culture conditions. It has been indicated that engineered scaffolds with discrete or continuous gradient properties are superior to single-phase tissue scaffolds for OC defect repair [14,15]. Some studies developed discrete gradient scaffolds by fabrication of two or three phases separately, which are subsequently integrated with suturing, glue, or press-fitting;

however, most of these scaffolds exhibit insufficient bonding strength, which raises the risk of phase delamination after implantation [18,19]. Other studies [16,17] proposed a continuous gradient scaffold with the freeze-drying approach; the scaffold structure changed in a linear gradient manner in terms of pore size and porosity. This design is less prone to delamination and can facilitate stress transfer within the scaffold. The continuous gradient scaffold has the potential to provide a smooth transition between cartilage and bone; moreover, it can avoid instability at the interface and better mimic the natural structure of the OC tissue. Although the development of OC tissue scaffolds has yielded good results in terms of OC regeneration *in vitro* or *in vivo,* longer-term follow-up clinical studies were not as satisfactory; further studies into gradient tissue scaffolds for OC regeneration are required.

Many types of scaffolds have been created by conventional methods such as solvent-casting [20,21], gas-forming [22,23], freeze-drying [24-27], and electrospinning [28-30] since these approaches offer flexibility in terms of selection of biomaterials as well as control over scaffold pore size and porosity. Recently 3D printing methods have been used for the OC scaffold fabrication due to their ability to fabricate interconnected porous scaffolds with well-controlled pore geometries; the scaffold structure may be designed to exhibit appropriate mechanical properties that match the host tissue. Various 3D printing techniques, including liquid, powder, and solid-based methods, have been used to create gradient scaffolds with several types of biomaterials, structural features, and mechanical properties for OC tissue regeneration [8-13]. Additionally, biological experiments have been used to investigate cell response in a dynamic cultural environment. For instance, physical stimuli such as mechanical strain and fluid shear stress from compressive loading as well as fluid flow within bioreactors have been investigated for enhancing tissue regeneration [31-33]; however, it is time-consuming and costly to evaluate the many parameters that affect tissue regeneration *in vitro* or *in vivo*. Computational modeling

shows excellent potential in biomedical engineering research; for example, data from modeling and experiments can be used to understand the correlation between physical stimuli and cellular responses for bone and cartilage formation.

In this review, the gradient characteristics of OC tissue in terms of biochemical composition, structure, and mechanical properties are considered. Approaches for tissue engineering of gradient OC tissue scaffolds are considered; the use of various cell types, growth factors, scaffold materials, structures, mechanical properties, fabrication methods, and physical stimuli under various culture conditions are considered. We highlight recent developments in gradient OC scaffolds using 3D printing techniques, the application of computational modeling in scaffold structure design. Challenges associated with the repair of OC defects and recommendations for future directions are considered in the final section of this review.

2 Biochemical composition, structure, and mechanical property of OC tissue

OC tissue is composed of two main components, cartilage and bone. As shown in Figure 1 A, OC tissue exhibits a transition from hard bone to soft cartilage; this transition exhibits gradient characteristics. The cartilage can be further divided into calcified cartilage and noncalcified cartilage; the “tidemark” serves as the interface between noncalcified cartilage and calcified cartilage. The natural OC tissue gradient is defined by changes in the biochemical composition, structure, and mechanical properties from the surface of the cartilage to the subchondral bone. The properties of the cartilage, calcified cartilage, and subchondral bone components are summarized in Table 1.

The noncalcified cartilage contains three zones, which are the deep zone (on top of the calcified cartilage (30-40%)); the middle zone (centrally located in noncalcified cartilage tissue (40-60%)); and the superficial zone (interfacing with the synovial fluid and the joint surface (10-20%)) [34,35]. Cartilage is mainly composed of water (60%-80%), extracellular matrix components (mainly collagen II fibers), and chondrocytes [36]. The diameter and orientation of collagen fibrils vary from the superficial zone to the deep zone of cartilage. The superficial zone contains the thinnest collagen fibrils (30-35 nm), which are arranged in a highly parallel orientation to the joint surface. The collagen fibrils diameter increases in the middle zone of cartilage; fewer parallel arrangements are observed in the middle zone than in the superficial zone. The diameter of collagen fibrils is 40-80 nm in the deep zone of cartilage; the fibrils are oriented perpendicular to the joint surface to enhance the strength of the bonds between the cartilage and the bone [37]. The superficial zone contains the largest number of chondrocytes; these cells exhibit flattened morphologies and alignment parallel to the joining surface in the superficial zone. In the middle zone, chondrocytes exhibit a rounded shape and a lower number of cells. The fewest number of chondrocytes appear in the deep zone; in this zone, the cells exhibit rounded and ellipsoid shapes [37,38].

+

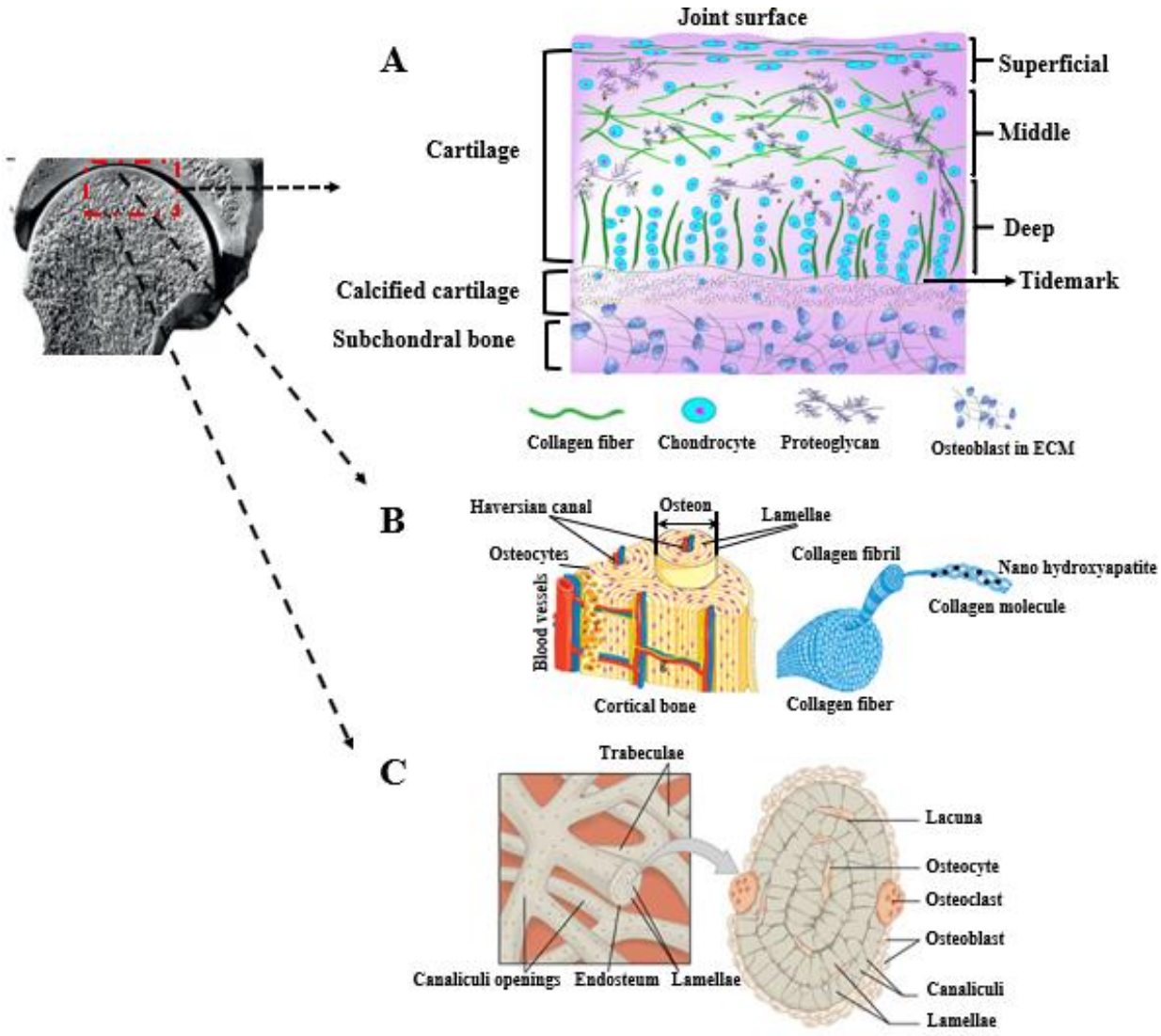

Figure 1. Images of the gradient characteristics of natural OC tissue. (A) A schematic diagram of the OC unit, which includes cartilage, calcified cartilage, and subchondral bone [37]. Reprinted from ref. 37 with permission from the CRC Press, Copyright 2011. (B) The material composition of cortical bone tissue [39]. Reprinted from ref. 39 with permission from Springer Nature, Copyright 2015. (C) The material composition of trabecular bone tissue [40]. Reprinted from ref. 40 with permission from OpenStax, Copyright 2013.

Table 1. The gradient biochemical composition, structure, and mechanical property of OC natural tissue.

	Biochemical composition		Structure	Mechanical property
	Cells	Materials		
Cartilage [15,26,41,42]	Chondrocyte morphology is flattened in the cartilage surface zone and gradually becomes a round and ellipsoid shape in the deep zone	Type II collagen fibrils are parallel to the joint surface in the cartilage surface zone and gradually become perpendicular to the joint surface in the deep zone	Cartilage is a highly interconnected tissue with a porosity of 60%-85% and a pore size of 2-6 nm	The compressive modulus of cartilage increases from the superficial to the deep zone from 0.2 to 6.44 MPa
Calcified cartilage [43-45]	Chondrocyte size in calcified cartilage is higher than in cartilage	Collagen fibrils are anchored to the subchondral bone and hold the cartilage and subchondral bone	Calcified cartilage is located in the transition zone from cartilage and bone; its pore size and porosity gradually vary	The compressive modulus values of cartilage, calcified cartilage, and bone exhibit anisotropic properties and vary in a depth-dependent manner`
Subchondral bone [46-50]	Osteoblasts, osteoclasts, osteocytes, and MSCs	Hydroxyapatite crystalline plate-shaped particles with length of 20-50 nm, width of 15 nm, and thickness of 2-5 nm are deposited on type I collagen fibrils	Subchondral bone contains cortical bone (top) and trabecular bone (bottom). The pore size varies from 0.1-2000 μm and the porosity changes from 5-90% from the top to the bottom of the subchondral bone	Compressive modulus values for cortical bone and trabecular bone are 18-22 GPa and 0.1-0.9 GPa, respectively

Calcified cartilage is located in the transition region of OC tissue; it contains fewer chondrocytes than the noncalcified cartilage zones. The collagen fibrils in this zone are anchored to the subchondral bone and serve to hold the cartilage and subchondral bone. Features of bone tissue (e.g., the presence of alkaline phosphatase) can be found in the calcified cartilage zone [51,52]. Below the calcified cartilage is subchondral bone, which contains cortical bone and trabecular bone. The material composition of this layer is shown in Figure 1 B and C. The cortical bone locates immediately underneath the calcified cartilage, whereas the trabecular bone is below the cortical bone. Bone is composed of water (10%), organic components (30% - mainly collagen I), and mineral components (60% - mainly hydroxyapatite (HAp)). The HAp crystalline nanoparticles, which exhibit a plate shape with a thickness of 2 - 5 nm, a length of 15 - 150 nm, and a width of 10 - 80 nm, are located on the collagen I fibrils (30 - 300 nm) [39,53,54]. The cells in the bone tissue include osteoblasts, osteoclasts, osteocytes, and mesenchymal stem cells (MSCs). Osteoblasts are the cells that form new bone; these cells are also responsible for HAp synthesis. Osteoclasts are associated with bone resorption. Osteocytes are the most common cell type in bone; they regulate the interaction between osteoblasts and osteoclasts. MSCs are multi-potential stromal cells that are able to differentiate into many cell types such as osteoblasts and chondrocytes [55].

The structure and mechanical properties of the OC tissue vary from the surface of the cartilage to the subchondral bone. The cartilage within OC tissue has a gel-like structure with the porosity of 60-85%; the cells in the articular cartilage are fed by articular fluid that moves across the cartilage pores. The cortical bone has high stiffness; its porosity ranges from 5% to 30%. The stiffness decreases from the cortical bone to the trabecular bone as the porosity increases; the porosity of trabecular bone ranges from 30% to 90%. Porous structures in the subchondral bone tissue are filled with vessels and nerve fibers that provide bone cells with

nutrients and remove waste [15,22,56]. The mechanical properties of OC tissue vary from cartilage to subchondral bone; this variation is primarily associated with changes to the material composition and structure. The compressive modulus of cartilage shows a depth-dependent change due to variations in the cellular and molecular composition from the superficial zone to the deep zone. The compressive modulus and compressive strength of cartilage gradually increase from the superficial to the deep zone; the compressive modulus increases from 0.2 to 6.44 MPa, and the compressive strength increases from 0.005 to 4 MPa [15,57-59]. Bone tissue consists of organic and inorganic components; the arrangement of these organic and inorganic components gives bone tissue its anisotropic properties. For instance, the transverse elastic modulus and longitudinal modulus of cortical bone are 10.1 ± 2.4 GPa and 17.9 ± 3.9 GPa, respectively. The tension and compression strength of cortical bone in the longitudinal direction are 135 ± 15.6 MPa and 205 ± 17.3 MPa, respectively; the tension and compression strength of cortical bone in the transverse direction are 53 ± 10.7 MPa, and 131 ± 20.7 MPa, respectively [60]. Trabecular bone performs better under compression than tension, and its compressive elastic modulus and compressive strength are range from 1 - 900 MPa and 1 - 10 MPa, respectively [42,56,57,61-63].

3 OC tissue defects

OC defects often include the destruction of articular cartilage and alterations to the underlying subchondral bone. Heinegård *et al.* compared the matrix in healthy OC tissue and osteoarthritis-affected defected OC tissue (Figure 2 A and B) [64]. The cartilage compartments in the defect-containing OC tissue exhibit cloning and multiplication of cells at the early stages. This phenomenon results in cartilage destruction, thicker subchondral bone, and decreased trabecular volume. The immunohistochemistry staining data indicate that the degradation of the interterritorial matrix (solid arrow) and changes to the pericellular matrix (dashed arrow)

in the cartilage. Those changes in the cartilage and the underlying subchondral bone can lead to chronic pain and dysfunctional joint movement.

The current surgical treatments for OC defects depend on the lesion size and severity (Figure 2 C). Microfracture is often used for the treatment of cartilage defects smaller than 1 cm^2; this approach stimulates MSCs from subchondral bone to repair cartilage tissue [4]. Autograft or allograft is used to treat lesions in the range of 1 - 4 cm^2 [65]; a total joint replacement is required for severe degeneration [3]. While these treatments are evolving, the limitations of conventional treatments continue to spur the development of new therapies. The drawbacks of conventional treatments include the quality and consistency of the tissue obtained from microfracture [66], limitations to the supply of autograft tissue, and the possible risk of microbial transmission from allograft tissue [6,7,67], as well as wear and loosening of prostheses [68,69]. Tissue engineering therapies are attractive due to their potential to create biological substitutes that can maintain, replace, or regenerate OC tissue [22].

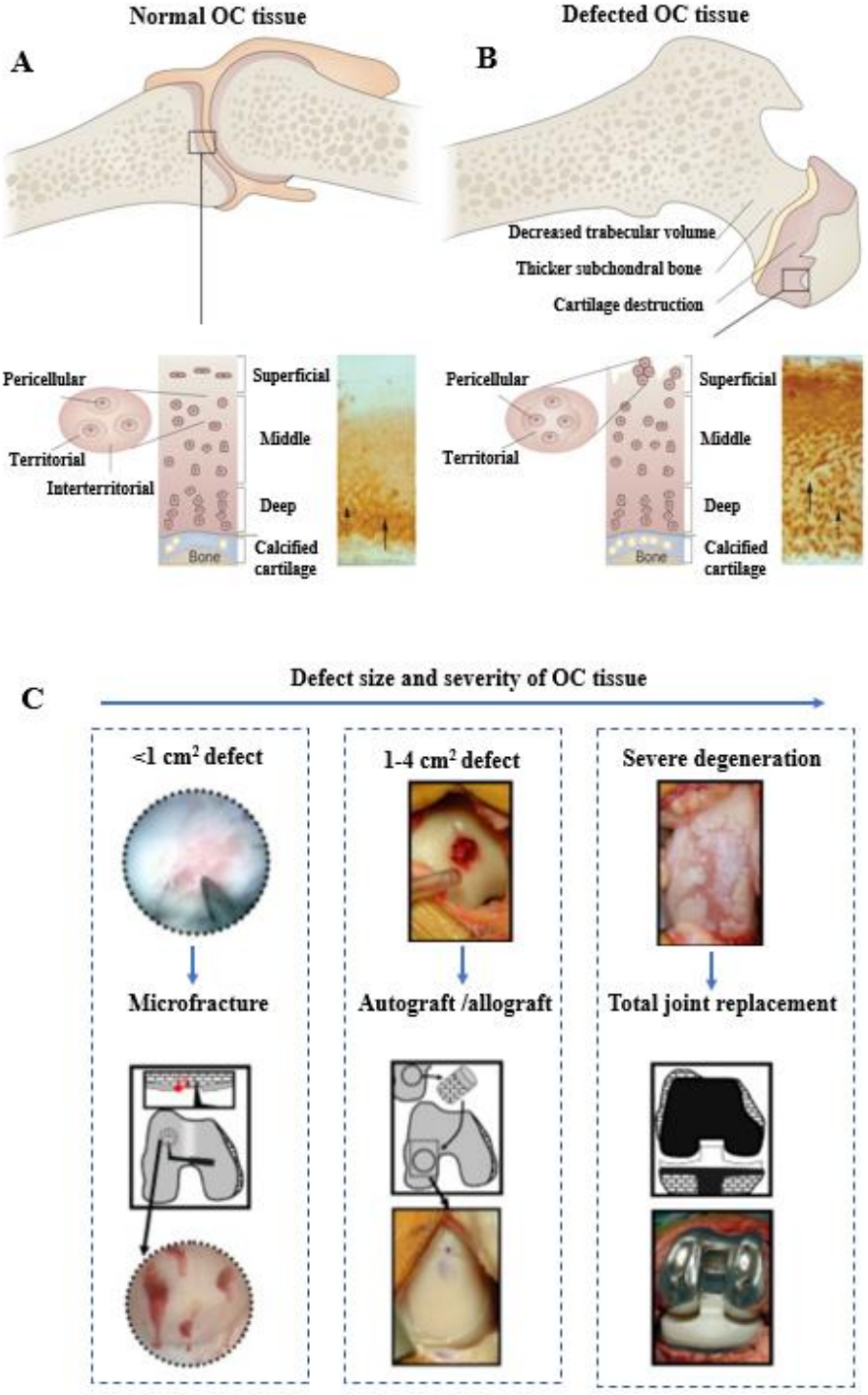

Figure 2. (A) A healthy OC tissue with normal cartilage, which is organized into pericellular, territorial, and interterritorial matrices. The immunohistochemistry results show that there was no cartilage oligomeric matrix protein present in the territorial and pericellular matrices (black dashed arrow). Interterritorial matrix staining showed the presence of the cartilage extracellular matrix molecule (solid black arrow). (B) A defected OC tissue in the osteoarthritic joint that shows partial loss of cartilage, subchondral bone thickening, and a decrease in trabecular bone volume. There were alterations in the cartilage compartments from cell cloning and multiplication. The immunohistochemistry results showed the loss of cartilage oligomeric matrix protein in the interterritorial matrix (solid black arrow); there was new synthesis of the molecule in the pericellular matrix of cartilage (black dashed arrow) [64]. Reprinted from ref. 64 with permission from Springer Nature, Copyright 2010. (C) Current clinical treatment options for OC defects [69]. The treatment options depend on defect size and severity. Reprinted from ref. 69 with permission from Elsevier, Copyright 2009.

4 Tissue engineering for OC tissue regeneration

The biochemical composition, structure, and mechanical properties of natural OC tissue exhibit a gradient transition from the surface of the cartilage to the subchondral bone. To closely mimic the gradient transition of OC tissue, the cell type [70-72], growth factor [73-75], scaffold material [8,76,77], scaffold structure [75,78,79], mechanical properties [10,56,80], and culture conditions must also exhibit a gradient transition [31,33,81]. The fabrication methods for gradient OC tissue scaffold are introduced, and the application of 3D printing techniques for OC scaffold fabrication was considered. 3D printing techniques enable control over the pore geometry within the scaffold to obtain scaffolds with appropriate mechanical properties for OC tissue repair.

4.1 Cells, growth factors, and material composition in OC tissue engineering

Tissue engineering typically involves the use of porous tissue scaffolds in which cells can adhere, proliferate, differentiate, and migrate to enable tissue regeneration. Although it may be possible to use cell-free scaffolds to repair OC tissue containing minor defects, the scaffold alone cannot usually initiate appropriate biological responses for OC tissue regeneration [70]. Cells used for the OC tissue repair, either *in vitro* or *in vivo*, include chondrocytes, osteoblasts, and MSCs. Chondrocytes and osteoblasts are often seeded in separate layers of the cartilage and bone components of the OC tissue scaffold. However, the limited presence of chondrocytes in natural OC tissue (around 5% of total cartilage volume) restricts the application of chondrocytes in OC tissue engineering. Additionally, the isolation of collagen from the extracellular matrix (ECM) requires the use of collagenase, which can harm the chondrocytes. It has also been suggested that chondrocytes lose appropriate phenotypic expression in the culture environment [71]. MSCs have been used for OC tissue regeneration since they have the capability to differentiate into chondrocytes and osteoblasts; MSCs are seen as an alternative

to overcome the limited supply of chondrocytes [72]. In addition, growth factors play an important role in directing MSCs differentiation into target cells. The sequential addition of growth factors to a scaffold is useful for stimulating chondrogenesis; for instance, chondrocytes seeded in agarose gels to transforming growth factor-beta 3 (TGF-β3) for two weeks showed better cartilage formation and mechanical properties than chondrocytes seeded in agarose gels without TGFβ3 [82]. Similarly, the exposure of MSCs in poly(ethylene glycol) (PEG) hydrogels to TGF-β1 resulted in enhanced proliferation and proteoglycan production [83].

Abrahamsson *et al.* fabricated polycaprolactone (PCL) tissue scaffolds, seeded the scaffolds with human MSCs, and cultured the scaffolds in a medium containing human TGF-β3 [84]. The formation of cartilaginous tissue was observed after culture for 21 days *in vitro*; moreover, the construct showed mechanical properties similar to those of native articular cartilage after culture for 45 days. Similarly, the use of growth factors is important for osteogenesis. The most commonly used inducing factor for osteogenesis is bone morphogenetic protein-2 (BMP-2), which is usually immobilized on scaffolds to promote osteoblast differentiation [73,85]. Additionally, calcium phosphate and HAp nanoparticles are used as osteogenic regulators in tissue engineering; these materials promote osteogenic differentiation of MSCs and change the physical properties of the scaffold [74,85]. Porous alginate constructs incorporating the osteogenic growth factor BMP2 and calcium phosphate particles were able to efficiently transfect encapsulated MSCs over fourteen days and promote their differentiation towards the osteogenic lineage [85]. In general, chondrogenic growth factors (e.g., TGF-β family) supplied to the cartilage layer of the OC scaffold are beneficial for chondrogenesis. Osteogenic growth factors (e.g., BMPs or HAp nanoparticles) are incorporated within the bone layer of the OC scaffold for osteogenesis [71].

A range of biocompatible materials, including natural polymers, synthetic polymers, inorganic materials, and metallic materials, have been used to fabricate OC tissue scaffolds. Natural polymers such as collagen, gelatin, chitosan, alginate, and silk have been used for OC scaffold fabrication because of their similarity to the structure of extracellular matrix and their biocompatibility [77,86,87]. Collagen is the most commonly used natural polymer for OC scaffold fabrication since it is the main component of connective tissue; however, it is unstable. Due to its rapid degradation rate, the scaffold is unable to maintain structural integrity. Crosslinking treatments can be performed to extend the durability and mechanical strength of this material [88,89]. Gelatin has also been used for cartilage repair due to its low cost and facile preparation; due to its poor mechanical properties, gelatin is usually used in combination with other materials such as HAp, bioactive glass, and chitosan. Silk materials have also been for OC scaffold since they are stable, flexible, and highly resistant in tension and compression [90]; the main disadvantage of silk is the very low speed of its production by spiders [91]. In general, although natural polymers closely mimic natural cartilage tissue, shortcomings such as limited supply, low stable, high degradation rate, and low mechanical strength limit their use for OC scaffold fabrication.

Synthetic polymers such as PCL, poly(lactic-co-glycolic acid) (PLGA), polyglycolic acid, PEG, polylactic acid, polydioxanone, and poly (propylene fumarate) have been used for the fabrication of OC scaffolds [92]. Since most synthetic polymers are hydrophobic, limitations in terms of cell attachment and differentiation may occur due to an insufficient number of interaction sites [76]. Blends of hydrophobic and hydrophilic polymers are sometimes used to enhance hydrophilicity and promote cell attachment [93,94]. Bioceramics such as HAp, tricalcium phosphate (TCP), and bioglass are capable of stimulating biomineralization for bone tissue repair; the biodegradability of calcium phosphate materials can be controlled by altering the

calcium-to-phosphorus ratio [46,95]. Although bioceramic based scaffolds have high bioactivity, they are brittle and cannot resist mechanical stresses; thus, scaffolds containing composites of natural or synthetic polymers and bioceramics may exhibit better mechanical properties than bioceramic scaffolds [46,96].

In order to mimic the gradient of cartilage, calcified cartilage, and bone within natural OC tissue, two main categories of scaffolds, discrete and continuous gradient scaffolds, have been developed (Figure 3). Discrete gradient scaffolds can be categorized as biphasic or tri/multiphasic. For a biphasic OC scaffold, individual bone and cartilage scaffolds can be joined together. As shown in Figure 3 A, Schaefer *et al.* fabricated a polyglycolic acid (PGA) scaffold for the cartilage layer and a PLGA/PEG scaffold for the bone layer; bovine calf articular chondrocytes and bone cells were seeded on those scaffolds separately. The two components were then sutured together. The *in vitro* results at two weeks show increased glycosaminoglycan (GAG) production on the cartilage side of the scaffold as well as apparent mineralization of the ECM on the bone side of the scaffold [19]. As shown in Figure 3 (B), Chen *et al*. developed a biphasic OC scaffold containing TGF-β1 activated chitosan/gelatin for the chondrogenic layer and BMP-2 activated HAp/chitosan/gelatin for the osteogenic layer. The structures were separately seeded with MSCs and fused with fibrin glue. The *in vivo* results indicate that the scaffold supported the regeneration of cartilage and subchondral bone after twelve weeks of implantation in a rabbit knee defect [97]. Zhao *et al.* fabricated porous PLGA and titanium (Ti) scaffolds; a pressing method was applied to join two scaffolds together to create a biphasic construct (shown in Figure 3 (C)). The *in vivo* results showed that there was better cartilage and subchondral bone repair in the PLGA/Ti biphasic scaffold than in the PLGA or Ti scaffold. Moreover, the tri/multiphasic scaffolds were shown to closely mimic the cartilage, bone, and transition zone of calcified cartilage in natural OC tissue [98]. Figure 3 (D)

shows tri-phasic scaffolds developed by Jiang *et al.*; PLGA and bioactive glass seeded with osteoblasts were used to create the bone layer. Agarose hydrogel seeded with chondrocytes was used to create the cartilage phase; the calcified cartilage phase was created using a combination of PLGA and agarose hydrogel. The *in vitro* results indicate that the appropriate tissue in each layer was formed; chondrocytes were observed within the calcified cartilage zone [99]. Figure 3 (E) shows multiphasic scaffolds prepared by Nooeaid *et al.*, which contain alginate for the cartilage layer, bioglass for the bone layer, an alginate/bioglass hybrid adhesive layer at the interface of cartilage and bone. The three layers were joined together by press-fitting manually. The results showed that the multiphasic scaffolds had appropriate porosity, pore size, and mechanical properties for use as an OC tissue scaffold [100]. Levingstone *et al.* developed a multiphasic scaffold; the construct contained three types of layers. As shown in Figure 3 (F), the bone layer was composed of type I collagen and HAp; the calcified cartilage layer was composed of type I collagen, type II collagen, and HAp. The cartilage layer was composed of type I collagen, type II collagen, and hyaluronic acid. The *in vitro* results involving this scaffold showed a homogeneous cellular distribution throughout the entire construct [24].

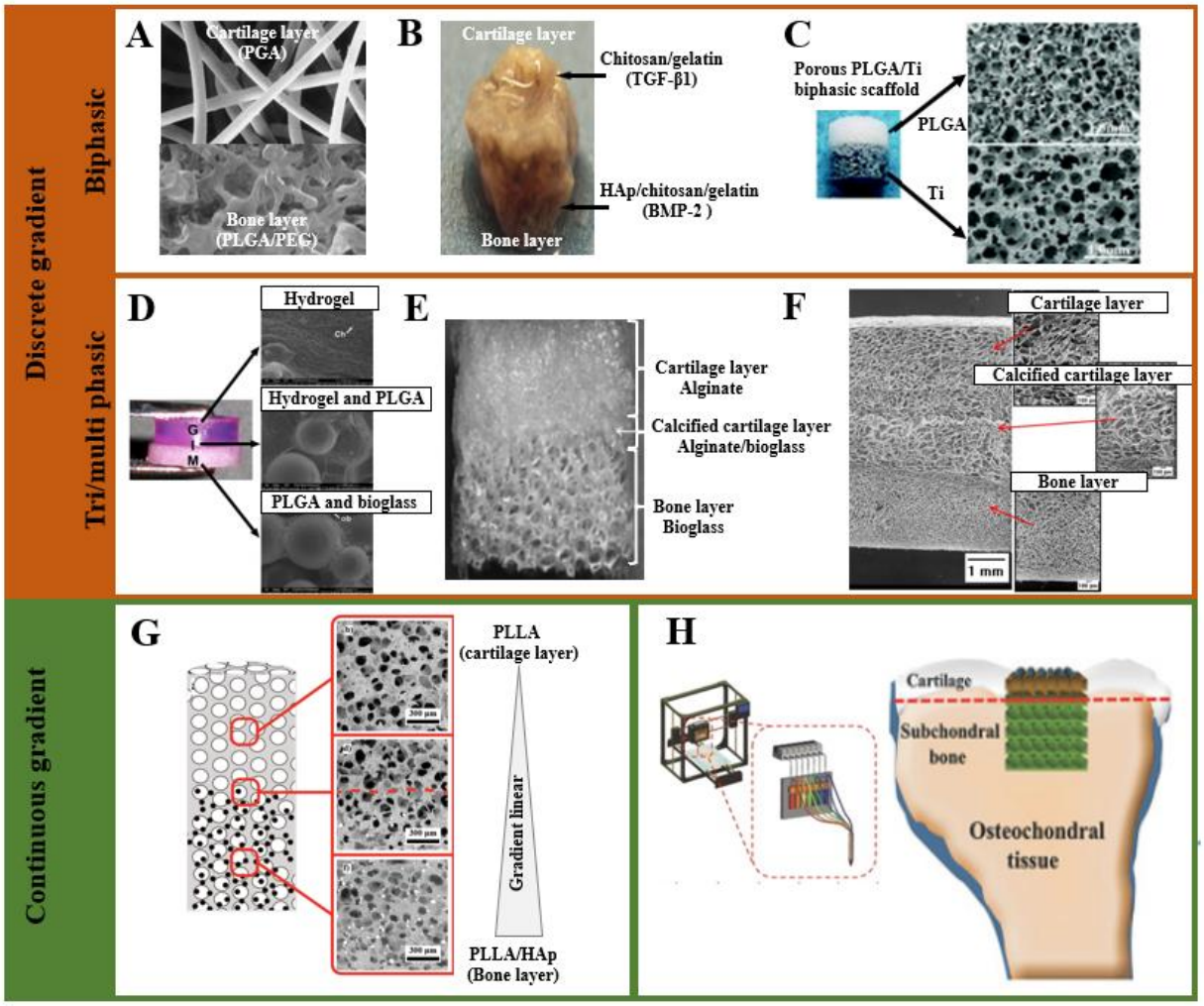

Figure 3. Discrete and continuous gradient scaffolds for OC tissue regeneration. (A) biphasic scaffold containing PGA and PLGA/PEG for the cartilage and bone layer, respectively [19]. Reprinted from ref. 19 with permission from Elsevier, Copyright 2000. (B) Biphasic scaffold made of chitosan/gelatin and HAp/chitosan/gelatin [97]. Reprinted from ref. 97 with permission from Elsevier, Copyright 2011. (C) Biphasic scaffold made by PLGA and porous Ti blocks [98]. Reprinted from ref. 98 with permission from the Royal Society of Chemistry, Copyright 2013. (D) Tri-phasic scaffold containing a cartilage phase consisting of agarose hydrogel, a calcified cartilage phase consisting of agarose hydrogel/PLGA/bioglass, and a bone phase containing PLGA/bioglass [99]. Reprinted from ref. 99 with permission from Springer Nature, Copyright 2010. (E) Tri-phasic scaffold with alginate as the cartilage layer, alginate/bioglass composite as the calcified cartilage layer, and bioglass as the bone layer [100]. Reprinted from ref. 100 with permission from John Wiley and Sons, Copyright 2014. (F) Tri-phasic scaffolds with a cartilage layer composed of type I collagen/type II collagen/hyaluronic acid, a calcified cartilage layer composed of type I collagen/type II collagen/HAp, and a bone layer composed of type I collagen/HAp [24]. Reprinted from ref. 24 with permission from Elsevier, Copyright 2014. (G) Continuous gradient scaffolds with PLLA in the cartilage layer and PLLA/HAp in the bone layer [101]. Reprinted from ref 101 with permission from IEEE, Copyright 2018. (H) Proof of concept of developing continuous gradient scaffold with bioinks using the 3D printing technique [75,102]. Reprinted from ref. 75, 102 with permission from John Wiley and Sons, Copyright 2018.

Researchers fabricated a continuous gradient scaffold to more closely mimic the gradient characteristics of OC tissue. Compared with discrete gradient scaffolds, the continuous gradient scaffold has the potential to induce a smooth transition between the cartilage and bone

component, avoiding instability at the interface. Dormer *et al.* developed continuous gradient PLGA scaffolds using programmable pumps to control the flow rate; they created a gradient in terms of microsphere size and distribution. The top quarter and the bottom quarter of the scaffold contained TGF-β1 and BMP-2, respectively; the transition region from TGF-β1 to BMP-2 constituted the middle half of the scaffold. MSCs were seeded on the gradient scaffold; the *in vitro* results showed that there was improved GAG production and alkaline phosphatase activity [17]. La Carrubba *et al.* created poly-l-lactic acid/HAp scaffolds with a continuous gradient in microsphere size and distribution. The HAp concentration was gradually increased from the cartilage region to the bone region within the scaffold (Figure 3 (G)) [101]. Parisi *et al.* developed a continuous gradient scaffold using a freeze-drying process by varying the ratio of collagen to HAp from the bottom to the top of the scaffold; the bottom of the scaffold had the highest HAp content, and the top of the scaffold had no HAp. Physicochemical studies were used to examine the chemical composition and the distribution of mineral in the scaffold. By changing the biomaterial composition from the cartilage region to the bone region, the mechanical properties of the scaffold were modulated in a gradient manner. The *in vitro* results show that the composition and stiffness gradients increased cell proliferation in different sub-regions of the scaffold according to their chondrogenic or osteogenic characteristics [27]. As shown in Figure 3 (H), a 3D printing method was used to develop a continuous gradient scaffold for OC tissue repair. A scaffold with the desired gradient was prepared with independent or simultaneous control over more than seven distinct bioinks [102]. Details about the use of 3D printing for OC tissue scaffold processing are described in Section 4.3.2.

4.2 Structure and mechanical properties in OC tissue engineering

An efficient OC scaffold design should provide a porous gradient structure with appropriate mechanical properties to match with the host tissue. The scaffold pore size should be larger than the dimensions of the relevant cells so that the cells can readily migrate into the scaffold;

the pore size and porosity have significant effects on chondrogenesis and osteogenesis. A scaffold structure with a porosity higher than 50% and pores larger than 300 μm is recommended to achieve direct osteogenesis with enhanced vascularization [103]. On the other hand, 90 - 120 μm pores are favorable for chondrogenesis (e.g., MSC proliferation and cartilage tissue formation on the scaffold) [104]. This difference in pore size is attributed to the fact that bone and cartilage tissue exhibit different levels of metabolism activity. Since oxygen is supplied mostly by the synovial fluid on the surface of the cartilage, chondrocytes consume a lower amount of oxygen than other cell types. While oxygen for subchondral bone is supplied by blood vessels, the pore size of the bone scaffold should enable the growth of blood vessels in the scaffold for exchanging nutrients, oxygen, and metabolic waste [105].

Many studies discussed balancing the relationships among scaffold pore size, porosity, cell penetration, nutrient supply, and the mechanical properties of the scaffold. When scaffold pore size and porosity increase, cell penetration and nutrient supply generally show an increase. However, the scaffold mechanical strength decreases when the pore size and porosity increase (Figure 4 A). Wang *et al.* fabricated bi-layered scaffolds with cartilage ECM and HAp; various scaffold pore sizes and porosities were obtained by optimizing the HA/cartilage ECM ratio. The scaffold pore size decreased from 128.2 ± 20.3 μm to 21.2 ± 3.1 μm with the addition of HAp. The addition of HAp to the cartilage ECM construct increased the compressive modulus but decreased the permeability of the chondrocytes [106]. Korpayev *et al.* developed a chitosan/collagen/HAp based continuous gradient scaffold using freeze-drying; the HAp content in the scaffold was decreased from the bottom to the top of the scaffold. The top layer of the scaffold contained chitosan/collagen; no HAp was present on the top layer. The pore size varied along the vertical axis; the elastic modulus for the bottom layer exhibited the highest modulus value of 42.95 KPa [26]. Xiao *et al.* fabricated a silk fibroin/chitosan/HA scaffold in

which the HAp concentration increased gradually from the upper part of the scaffold to the lower part of the scaffold. The pore size gradually decreased from 152.6 μm to 74.66 μm in this scaffold [107]. Shi *et al.* fabricated a gradient alginate/dopamine/HAp scaffold using the freeze-drying technique; its porosity increased between the bottom and the top from 70.5% to 77.5%. The bottom layer in this scaffold contained the highest amount of HAp [25]. Apart from the scaffold pore size and porosity, pore interconnectivity is a critical factor for OC tissue. The interconnections between pores should be suitably large to support cell migration, proliferation, and subsequent ECM infiltration; as such, pore interconnectivity is a more important parameter than pore size. Scaffolds should ideally have a 100% interconnecting pore volume, which maximizing the exchange of nutrients and metabolic waste throughout the entire scaffold pore volume [15,108].

The scaffold material stiffness also influences cell morphology, attachment, and differentiation. Figure 4 B shows changes in the cell shape and differentiation of native MSCs that are directed by materials with different elasticities. Metal-polymer [98] and ceramic-polymer [97,99] compositions have been used to create structures with gradient mechanical properties. Metal alloys (e.g., Ti alloy), ceramics (e.g., HAp and TCP), and bioglass are used for bone regeneration; the polymers (e.g., PLGA, PCL) and alginate are used for cartilage regeneration. Piezoelectricity has been used for transduction of mechanical loading into electrical energy, which affects tissue regeneration. After placement of the scaffold at the OC tissue site, the dipole moments of the scaffold materials may be altered, creating an electric charge on the surface of cells. The signal reaches the cell membrane and activates calmodulin, calcineurin, and nuclear factor, which leads to the expression of genes for bone or cartilage production (e.g., cartilage--related gene expression of TGF-β and bone-related gene expression of BMP-2) [15].

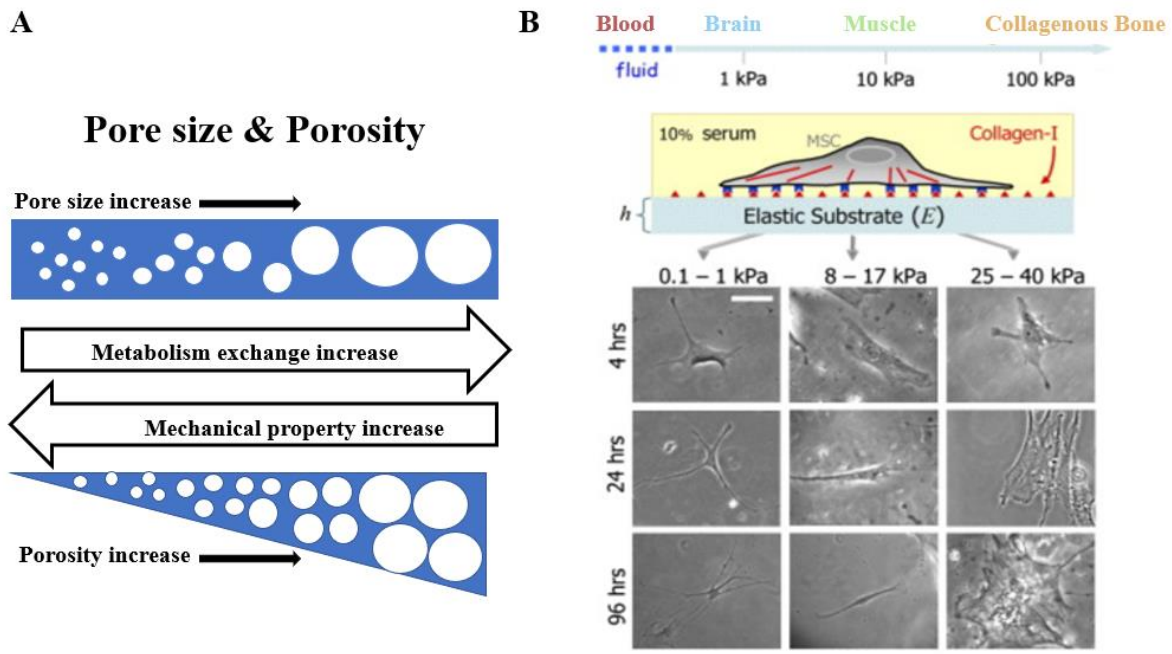

Figure 4. (A) Schematic images showing an optimal level of porosity and maintenance of high mechanical strength in a tissue scaffold. (B) The effect of material stiffness on cellular adhesion, differentiation behavior, and cell shape; the cells show small, branched, and spindle shapes. The scale bar is 20 μm [109]. Reprinted from ref. 109 with permission from Elsevier, Copyright 2006.

4.3 Fabrication methods in OC tissue engineering

The fabrication methods used to create OC tissue constructs can be divided into conventional and 3D printing methods. Conventional techniques of scaffold fabrication are generally cost-effective methods that provide some control over scaffold porosity and pore size; 3D printing techniques allow for independent control over macroscale and microscale features as well as enable the development of customized tissue scaffolds.

4.3.1 The application of conventional methods for OC scaffolds

Conventional fabrication methods such as solvent casting, gas forming, freeze-drying, and electrospinning have been used to create many types of OC tissue scaffolds [20,22,23]. In solvent casting, a solvent combined with uniformly distributed particles of a certain size is used to dissolve the polymer solution. The matrix is then submerged in the solvent; the particle is leached away to form a structure with porous features. It is a relatively straightforward and

low-cost technique that able to prepare scaffolds with porosities between 50% and 90% [20]. Researchers have used this technique to create OC scaffolds out of a combination of synthetic polymers [21,110]; bioactive compounds may be incorporated within the scaffold using this technique [111]. One of the drawbacks of solvent casting is that this approach is compatible with thin membranes or 3D specimens with very thin wall sections; in other cases, it is not possible to remove the soluble particles from within the polymer matrix [20]. In the gas foaming technique, the polymer granules are plasticized due to the employment of a gas such as nitrogen or carbon dioxide at high pressure. The advantage of the gas forming technique is that it enables the incorporation of heat-sensitive pharmaceuticals and biological agents within the scaffold. However, scaffold fabrication using gas forming is characterized by an incompletely interconnected pore network, which limits cell infiltration [23]. Gas forming in combination with particle leaching can provide a higher interconnected void network [22]. Freeze-drying of porous scaffolds is based on the conversion of frozen solvents into the gas phase; this approach can fabricate scaffolds with porosity greater than 90% and median pore sizes ranging from 15 to 35 μm (with larger pores greater than 200 μm); the scaffold pores exhibit relatively high interconnectivity. This technique has been used to create OC scaffolds out of natural polymers [24], synthetic polymers [17], and bioactive composites [25-27]. The freeze-drying method uses cytotoxic solvents; as such, the scaffold needs to be washed repeatedly to remove the solvent and minimize cytotoxicity [20]. Electrospinning is a technique for the fabrication of fibrous scaffolds, particularly scaffolds with a nanofibrous morphology. In this technique, a polymer solution ejected through a needle to form fibers under a strong electric field. Nanofibrous scaffolds can be modified by controlling the process parameters (e.g., voltage and fluid rate). Electrospinning fabricated scaffolds typically exhibit small pore sizes of less than 300 μm; these small pore sizes can hamper osteogenesis [28]. Post-fabrication procedures have been used

to make pores larger than 300 μm in electrospun scaffolds. For example, laser ablation has been used to generate pore sizes up to 500 μm [29,30].

4.3.2 The application of 3D printing methods for OC scaffolds

Three-dimensional (3D) printing has emerged as a new technology for OC scaffold fabrication. In 3D printing, a layer-by-layer fabrication process is guided by a computer-aided design model; excellent control over pore geometry is provided by this process. 3D printing enables fabrication of 100% interconnected pore structures and optimization of the mechanical properties of the scaffold [112]. Several 3D printing methods have been used to create tissue scaffolds. Three main categories of 3D printing techniques are used to create tissue scaffold, including solid-based (e.g., fused deposition modeling), powder-based (e.g., selective laser sintering and selective laser melting), and liquid-based (e.g., inkjet printing, stereolithography, 3D bioprinting and direct ink writing) techniques. The 3D printing techniques that are used to create OC scaffolds are summarized in Table 2.

Table 2. The application of 3D printing technologies for fabrication of gradient OC scaffolds to be used in OC tissue repair.

	Techniques	Scaffold materials	Scaffold structure	Gradient approach	*In vitro*/*in vivo* testing	Advantages/disadvantages
Solid-based 3D printing methods [79,113]	Fused Deposition Modelling	PCL	Woodpile structure with pore size gradients on the vertical direction	Pore size/porosity	The osteogenic lineage was improved in gradient scaffolds compared with non-gradient structures	+: Easily fabricate physical gradients -: Cannot incorporate cells or bioactive molecules during the printing
		Poly(ethylene glycol)	Pore size gradient lead to varying porosity in layers of scaffolds	Pore size/porosity	MSCs adhesion and proliferation on the 3D printed scaffolds with gradient pore size structures were improved when compared to uniform porous structures	
Powder-based 3D printing methods [78,114]	Selective Laser Sintering	PCL/HAp; HAp gradient change from the cartilage layer to the bone layer	A cylindrical scaffold with the pore size of 500 μm	Material composition	The gradient scaffolds induced the formation of cartilage and accelerated early subchondral bone regeneration in rabbit model *in vivo*	+: No support structures and toxic solvents required −: Cannot achieve horizontal compositional gradients
	Selective Laser Melting	Ti_6Al_4V	Scaffolds with different pore shape (triangular, hexagonal and rectangular) and pore size (500 μm and 1000 μm)	Pore size and pore shape	The gradient changing pore size and shape enhanced human placenta-derived cells (hPDC) seeding. The *in vitro* results indicate that differentiation of hPDC was dependent on both pore shape and pore size	+: Building high quality and complex metal parts and a large range of metal materials −: High power consumption
Liquid-based 3D printing methods [74,75,115-117]	Stereolithography	PDLLA	A gradient in both porosity and pore size in the horizontal direction	Pore size/porosity	Gradients in pore size and porosity influence the distribution of seeded human articular chondrocytes and anisotropic adherent cell densities.	+: Can create high resolution and complex internal structures − The limited application of biomaterials

						Cannot achieve horizontal compositional gradients
	Inkjet Printing	BMP-2 and fibrin	Fibrin film	Growth factor	Provide proof-of-concept of engineering spatial control over stem cells fates by controlling the printed patterns of BMP-2 immobilized to fibrin	+ Can fabricate both cells and bioactive molecules gradient -: Only feasible for low viscosity materials
	Extruded bioprinting	Porous poly(ethylene glycol)-terephthalate–poly(butylene terephthalate) copolymer	Pore-size gradients by varying fiber spacing from 0.5 to 2.0 mm)	Pore size	Pore-size gradients promoted an inhomogeneous bovine chondrocyte seeding within the scaffold and affected the inhomogeneous distribution of GAG and collagen type II	+: Can print a wide range of materials Allow for the printing of cells/bioactive factors Can fabricate both physical and compositional gradients -: Cannot achieve complex scaffold structure -: Difficulties with regard to ink formulation
		The top layers of scaffold fabricated with the PNT and TGF-β1 hydrogel, while the bottom layers were loaded with PNT and β-TCP hydrogel	Filament deposition-based woodpile structure	Material composition	The gradient hydrogel scaffolds promoted the regeneration of both cartilage and subchondral bone *in vivo*	

3D printing techniques are driving a shift toward personalized scaffolds. For example, personal scans of joints can be converted into computer-aided design files, which are then used to design patient-specific scaffolds. Such personalized scaffolds will not only provide a continuous gradient between bone and cartilage but also provide a continuous transition between the scaffold and the host tissue [118,119]. During the layer-by-layer 3D printing process, it is possible to incorporate several types of living cells, growth factors, and biomaterials within a scaffold (Figure 5 A). As such, 3D printing provides a mechanism for recapitulating the gradient characteristics of the OC unit [118]. The gradient scaffold that fabricated by 3D printing includes the material gradient, the structure gradient, and the gradient of both material and structure. As shown in Figure 5 B, Gao *et al.* formulated poly(N-acryloyl glycinamide) / poly(N-[tris(hydroxymethyl) methyl] acrylamide) co-polymer hydrogel (PNT) bioinks; they fabricated a gradient scaffolds with the bioinks using a bioprinting method. The top layers of the scaffold contained a hydrogel with PNT and TGF-β1; the bottom layers of the scaffold contained a hydrogel with PNT and β-TCP. The *in vitro* results indicated that the incorporation of β-TCP improved cell proliferation and differentiation of hBMSCs. The *in vivo* animal study indicated that the gradient hydrogel scaffolds could promote the regeneration of both cartilage and subchondral bone [75].

The effect of scaffold structure on cellular response has also been investigated. Andrea Di Luca *et al*. studied the influence of the pore size gradient on the osteogenic differentiation of hMSCs in fused deposition modeling-processed PCL scaffolds (Figure 5 C). The results indicated that differentiation of hMSCs toward the osteogenic lineage in mineralization media was improved in gradient scaffolds structures than in scaffolds with non-gradient structures [113]. Nowicki *et al.* used fused deposition modeling to fabricate PEG/PEG–diacrylate scaffolds with isotropic and anisotropic pore distributions. The anisotropic structure was fabricated by varying the

porosity of the scaffold layers. The *in vitro* results show that there was enhanced hMSC proliferation and differentiation within anisotropic 3D printed scaffolds than the 3D printed scaffolds with isotropic porous structures [79]. Bittner *et al.* created PCL/HAp scaffolds with gradients of structure and materials (Figure 5 D). The structural gradient was created by changing the scaffold pore size from top to bottom using 0.2 mm, 0.5 mm, or 0.9 mm fiber spacing; the material gradient was created by changing the HAp concentration from 0 wt% to 30 wt%. Mechanical property analysis results indicated that the large pore size in the gradient scaffolds was more deformed than the other sections; in addition, the gradient scaffolds exhibited compressive moduli in the range of human trabecular bone [8].

Various 3D printing methods have their advantages and restrictions. For instance, fused deposition modeling be used to create a gradient structure; however, it is difficult to obtain a material gradient within the scaffold. Additionally, cells and bioactive molecules cannot be incorporated during the printing process due to the high processing temperature. Cells and bioactive molecules cannot be incorporated during selective laser sintering and selective laser melting processes, which involve sintering or melting of powder precursors. On the other hand, droplet-based and extrusion bioprinting processes may be used to process scaffolds containing growth factors and cells at ambient or human body temperature; however, it is difficult to fabricate scaffolds with complex pore geometries using these processes.

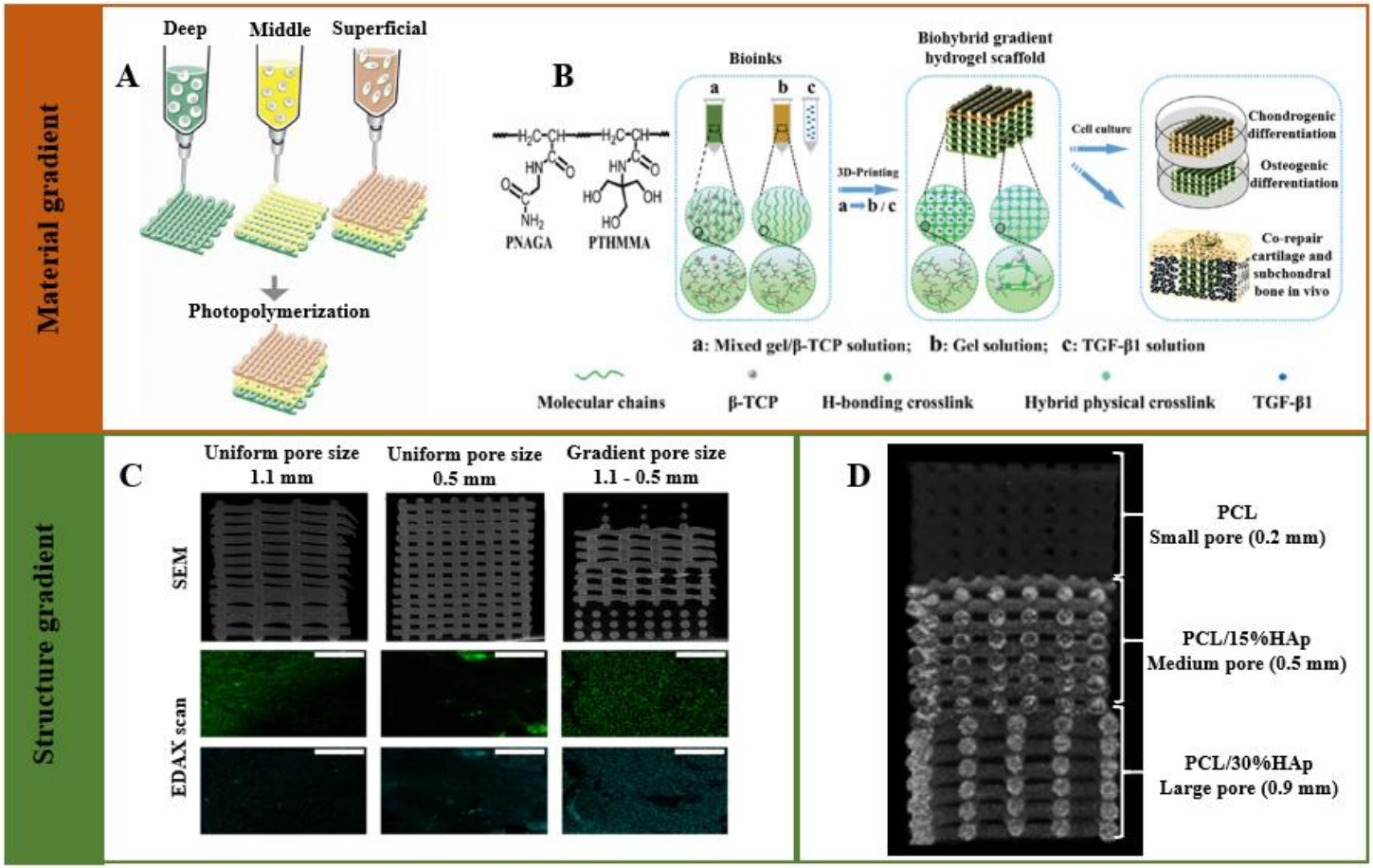

Figure 5. The application of 3D printing for a gradient OC tissue scaffold. (A) Schematic of the concept for 3D printing constructs in which chondrocytes from the deep, middle, and superficial zones are suspended in distinct hydrogel precursors and printed in defined geometries [118]. Reprinted from ref. 118 with permission from John Wiley and Sons, Copyright 2009. (B) Schematic illustration of the molecular structure and hydrogen bonding interactions in the PNT hydrogel and biohybrid gradient scaffolds produced with extrusion 3D printing [75]. Reprinted from ref. 75 with permission from John Wiley and Sons, Copyright 2018. (C) SEM image of a scaffold with pore sizes of 0.5 mm, 1.1 mm, and a gradient pore size from 1.1 to 0.5 mm; an EDAX scan at day 35 also shown, which reveals the presence of calcium (blue) and phosphate (green) in the scaffolds [113]. Reprinted from ref. 113 with permission from Springer Nature, Copyright 2016. (D) Gradient scaffold with material (HAp concentration) and structure (pore size change from 0.2-0.9 mm) [8]. Reprinted from ref. 8 with permission from Elsevier, Copyright 2019.

4.4 Culture conditions in OC tissue engineering

In addition to the scaffold materials, cells, growth factors, structures, mechanical properties, and fabrication techniques, the culture conditions used for OC tissue engineering need to be considered. Bioreactors are used to supply adequate nutrients and physical/mechanical stimuli for the cells that are seeded on the scaffolds. Perfusion bioreactors, which are considered more suitable for OC tissue engineering than other types of bioreactors, allow the flow of fluids through the pores of the porous scaffold. They are also capable of removing waste metabolites, including CO_2 and lactate [120].

He *et al.* fabricated a biphasic construct containing interfacing cartilage and bone scaffolds. As shown in Figure 6 A(a), a bioreactor was developed for perfusion of the medium through the bone region for five weeks; hMSCs were seeded in both compartments. Each culture system included medium containing either chondrogenic supplements or a mixture of chondrogenic and osteogenic supplements (Figure 6 A (b)). The medium flowed through the bone scaffolds at an inlet velocity of 400 μm/s. The results indicated that the formation of cartilage in the agarose gel region was negatively affected by the combination of perfusion and the mixture medium. On the other hand, the combination of perfusion and mixture medium enhanced bone formation in the biphasic scaffold [121]. Lin *et al.* designed a coculture bioreactor, which contained a perfusion bioreactor with a dual chamber. As shown in Figure 6 B (a), each chamber had one inlet and one outlet for chondrogenic medium (top) and osteogenic medium (bottom); the medium exchanged separately around the scaffold with the assistance of an O-ring. hMSCs were seeded on the cartilage scaffolds, which contained methacrylated gelatin and hyaluronic acid. hMSCs were also seeded on the bone scaffolds, which contained HAp instead of hyaluronic acid. The cell viability, cell proliferation, matrix production, and gene expression results indicated that the dual-chamber perfusion bioreactor positively influenced

the coculture of chondrocytes and osteoblast cells in the tissue engineering scaffolds. The junction between the sections of the scaffold exhibited GAG staining in the chondrogenic section and calcium staining in the osteogenic section (Figure 6 B (a) and (b)) [31].

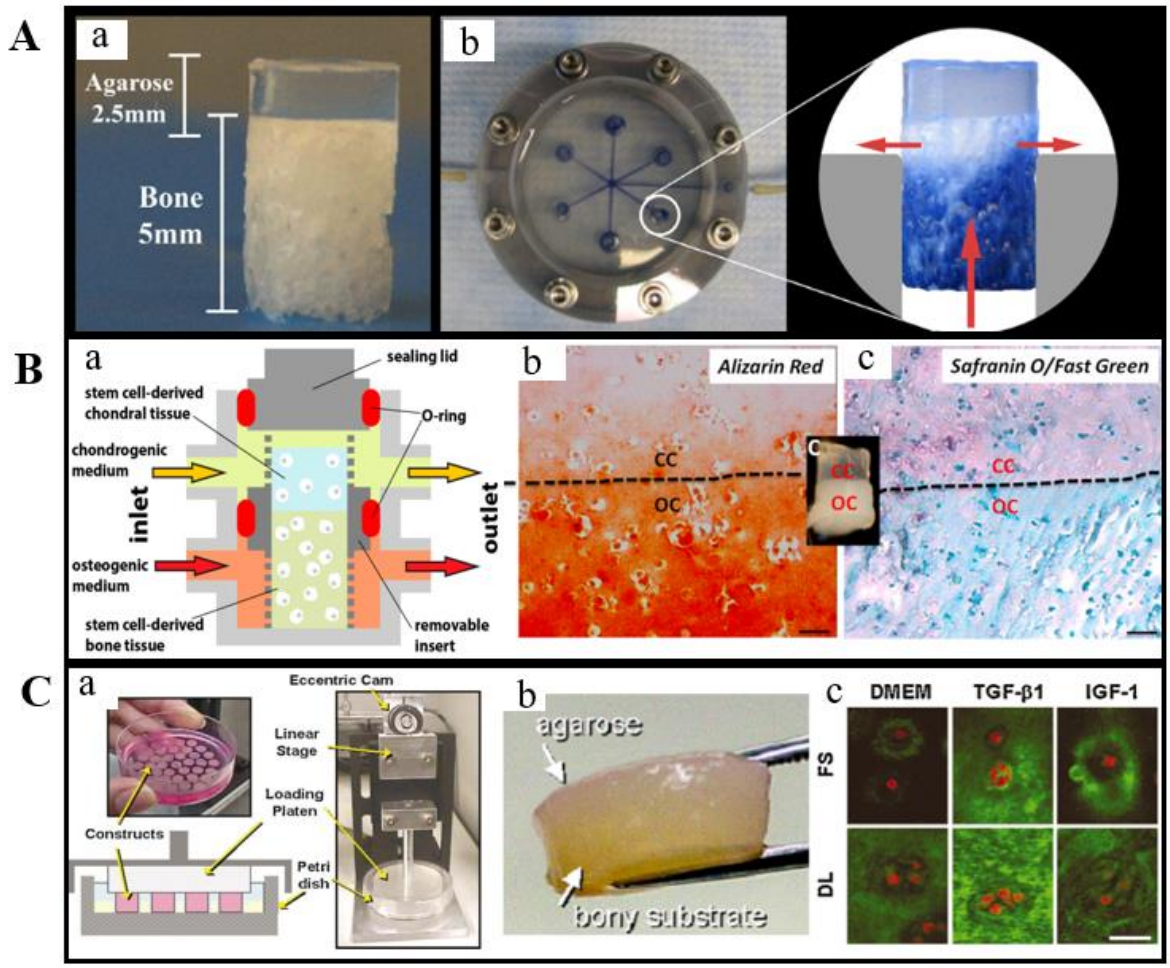

Figure 6. (A) Biphasic scaffold made by agarose and trabecular bone (a); perfusion bioreactor for the cultivation of biphasic scaffolds; enlarged view showing the medium flow path through the scaffolds and the reservoir (b) [81]. Reprinted from ref. 81 with permission from Elsevier, Copyright 2010. (B) Schematic illustration of the coculture perfusion bioreactor with two chambers, one inlet and one outlet for chondrogenic medium (top) and osteogenic medium (bottom) exchange (a); histology of the interfacial region for the chondral component and the osseous component. Alizarin red staining for calcium (b); safranin-O staining for negatively charged molecules (GAG), and fast green staining for proteins (c); scale bar = 100 μm [31]. Reprinted from ref. 31 with permission from American Chemical Society, Copyright 2014. (C) Bioreactor system for dynamic deformational loading; the construct underwent dynamic loading with 10% deformation (a); the scaffold was fabricated with bone and agarose (b) type II collagen staining of constructs after five weeks of culture in DMEM with supplements of TGF-β1 and IGF-1 under free swelling (FS) and dynamic loading (DL) conditions, scale bar = 20 μm [32]. Reprinted from ref. 32 with permission from Springer Nature, Copyright 2004.

The use of interstitial flow-induced fluid shear stress was examined in relation to cell differentiation for OC tissue repair. McBride *et al.* studied the effect of shear stress on gene expression changes in MSCs. They indicated that exposure of MSCs to continuous shear stress induced upregulation of ossification-related genes such as Runt-related transcription factor 2 (RUNX2) and SOX-9 [122]. Kreke *et al.* applied a shear flow (0.16 Pa) to MSCs that were cultured in a perfusion bioreactor. The results showed that shear stress stimulated the osteoblastic differentiation of MSCs; this finding was associated with an increase in alkaline phosphatase activity as well as expression of osteopontin, osteocalcin, and bone sialoprotein [123]. Lee *et al.* suggested that exposure to a low magnitude of shear stress (i.e., 0.03 - 0.27 Pa) induced osteogenic differentiation, including increased expression of osteocalcin [124]. Kim *et al.* applied shear flow to MSCs cultured in a perfusion bioreactor with flow stress in the range of 0.012 - 0.015 Pa. They found that fluid shear stress induced alkaline phosphatase activity and markers of osteogenic differentiation (e.g., RUNX2) [125].

Compressive loading is another critical factor that can affect cell response. As shown in Figure 6 C (a) & (b), Hung *et al.* fabricated a compressive loading bioreactor. The scaffold contained bone and agarose; chondrocytes were seeded on the bilayer scaffold. The immunofluorescent staining results for type II collagen indicated that the application of 10% compressive loading increased levels of cell biosynthesis products and enhanced their distribution [32]. Sumanasinghe *et al.* initially investigated hMSCs trapped in a 3D collagen matrix under strain (0% or 10%) for 7 and 14 days. The hMSCs subjected to 10% strain demonstrated a significant increase in BMP-2 mRNA expression compared to the hMSCs not subjected to strain after 7 and 14 days. They concluded that compressive strain was able to induce osteogenic differentiation without the addition of osteogenic growth factors [126]. Michalopoulos *et al.* seeded hMSCs on collagen alginate scaffolds and subjected the scaffolds to 10% or 15% compressive strain for up to 21

days. The results indicated that the hMSCs were able to differentiate into an osteogenic lineage, with an upregulated expression of core-binding factor alpha 1 under 10% strain. The cells were able to differentiate into a chondrogenic lineage under 15% strain alone, with increased expression of SOX-9 and aggrecan [127]. Pelaez *et al.* seeded MSCs in a fibrin gel that was subjected to 15% compression strain for 6 hours; they observed increased chondrogenic gene expression and deposition of glycosaminoglycans, indicating chondrogenic differentiation. The *in vitro* experimental results showed that strain was able to induce an increase in chondrogenesis and osteogenesis; osteogenesis of MSCs occurred at strain magnitudes lower than those for chondrogenesis [128].

In summary, a bioreactor system for the development of OC tissue contain two or three discrete compartments for the cells and the appropriate culture medium. Chondrogenic growth factor and compressive loading are required for the cartilage layers; osteogenic growth factor and interstitial flow are required for the bone layers to improve mass transfer.

4.5 Computational modeling application in OC tissue engineering

Biological studies have involved the development of bioreactors to optimize the physical/mechanical stimuli, the scaffold structure, and/or the materials, enabling optimal MSCs differentiation into chondrocytes and osteoblasts for OC repair. However, it is both costly and time-consuming to investigate the influence of each parameter on tissue regeneration *in vitro* or *in vivo*. Thus, computational modeling has been applied to predict the mechanical stimuli generated on scaffolds under specific culture conditions (i.e., compressive loading or fluid flow). The use of computational simulation methods together with biological experiments can facilitate a better understanding of the interactions among scaffold design, mechanical stimuli, and tissue regeneration.

4.5.1 Fundamentals of computational mechanobiology in OC tissue engineering

Various mechanic-regulation algorithms have been developed to describe the effects of mechanical stimuli on cells and tissues. Most recently developed mechano-regulation algorithms are based on a study by Pauwels *et al.* He proposed that two invariants of mechanical force guide cell differentiation-octahedral shear stress and hydrostatic stress. He noted that high hydrostatic stress induced chondrogenesis; on the other hand, high octahedral shear stress induced fibrous tissue formation [129]. Perren *et al.* investigated interfragmentary repair tissues; an interfragmentary strain theory based on the linear elastic behavior of tissue was proposed. The strain was defined as "the interfragmentary movement divided by the initial fracture gap size". They demonstrated that tissue differentiation is controlled by the resilience of callus tissues to strain. If the interfragmentary strain is higher than 10%, then only fibrous granulation tissue can form. If it is intermediate (2 - 10%), then cartilage is present; if it is lower than 2%, then bone formation occurs. However, the hypothesis only considered longitudinal strains; the strain contributions from radial and circumferential strains were neglected [130]. Carter *et al.* introduced a semiquantitative theory to define the contributions of the hydrostatic stress and the octahedral shear stress to tissue differentiation [131]. The octahedral shear stress was replaced by the octahedral strain in a subsequent study [132]. Claes *et al.* performed an *in vivo* study, which evaluated the thresholds of strain and stress values based on semiquantitative theory. They found that new bone formation in fracture healing mainly occurs along the existing bone edge. The results suggested that intramembranous bone formation occurs for hydrostatic stresses less than 0.15 MPa and strains lower than 5%. However, endochondral ossification was positively stimulated if hydrostatic stresses were greater than 0.15 MPa and strains were 5 - 15% [133].

The theories mentioned above all considered tissues as solid elastic materials. Prendergast *et al.* proposed a mechano-regulatory model for tissue differentiation based on the poroelastic behavior of tissues. They believed that stress on the cell was generated not only by tissue matrix deformation but also by the interstitial fluid flow within the scaffolds. High values of both solid strain and fluid shear stress cause fibrous tissue formation; on the other hand, intermediate values lead to cartilaginous tissue. Bone is formed only if the solid strain and fluid shear stress values are sufficiently low [134]. Huiskes *et al.* quantified the upper and lower limits of mechanical stimuli for various tissue phenotypes, and developed a mechano-regulatory model for tissue differentiation [135]. Over the past several years, the mechano-regulation theory has been used with finite element modeling to predict the influence of scaffold materials, scaffold structures, and culture conditions on cell migration and differentiation [136-138].

4.5.2 The application of finite element modeling in OC tissue engineering

The finite element (FE) modeling method has been used to predict the mechanical properties of 3D scaffolds; with the development of 3D printing techniques, scaffolds can be designed and analyzed with FE modeling, enabling researchers to explore the relationships among innovative scaffold topologies, mechanical properties, and tissue regeneration. It is particularly important to investigate OC tissue scaffolds with discrete or continuous gradient features that stimulate both cartilage and bone regeneration under mechanical loading or in a perfusion fluid bioreactor.

For example, FE modeling has been used for the analysis of scaffold mechanical properties under mechanical loading; Byrne *et al.* investigated the effects of scaffold porosity and dissolution rate under compressive loading on bone formation using the FE method based; a three-dimensional random-walk approach was utilized in this study. The results indicated that a high porosity and medium dissolution rate at a low loading site would result in the greatest

amount of bone regeneration; lower porosities and dissolution rates were recommended for a high loading site [138]. Melchels *et al.* designed CAD models with various structures (e.g., cube, diamond, and gyroid); they built the scaffolds out of poly(D, L-lactide)-based resin using the stereolithography approach. The bulk properties of the stereolithography produced solid materials were described mathematically using a constitutive model; the FE simulations results were compared with the mechanical testing experimental results. The results indicated that the gyroid structure provided a uniform strain distribution for cells within the scaffold, which would benefit cell growth and differentiation [139]. Several studies have been investigated the effects of various pore sizes and pore shapes on the mechanical properties of extrusion-printed OC scaffolds using the FE approach. For instance, Gleadall *et al.* compared the mechanical properties of two types of scaffolds with lattice and staggered filament arrangements under the same mechanical loading parameters; the Von Mises stress magnitude and distribution were analyzed. The FE results demonstrate that lattice structure formed a continuous pillar of filaments that help resist compression; the scaffold with staggered filaments compressed by deformation at hinge points, which were located at regions of high stress concentration. The staggered scaffold collapsed in a concertina manner by a slight bending of the filaments, which resulted in lower stiffness for the staggered scaffold than for the lattice scaffold with a continuous column of filaments [140]. Zhang *et al.* designed a scaffold in which the filament lay-down angle changed from 90^{o} to 15^{o} by moving from top to bottom (Figure 7 A). The FE analysis data for elastic modulus and compressive strength showed a gradient in loading in the *X, Y,* and *Z* directions (Figure 7 B); the maximum principal strain was decreased when filament the lay-down angle changed from 90^{o} to 15^{o} (Figure 7 C). The results indicate that the scaffold had anisotropic behavior and a gradient in mechanical properties in a depth-dependent manner; these results suggest that the hierarchical mechanical properties of natural OC tissue can be mimicked by tuning the porosity and local lay-down angles in 3D printed scaffolds [80]. Schipani

et al. investigated the effect of 3D printed scaffold geometry on the mechanical properties using the FE method. The results indicate that scaffolds with compressive properties spanning from the KPa to the MPa range can be obtained by varying filament diameter, spacing, and laydown pattern. The FE method combined with 3D printing represents a powerful approach to produce scaffolds that mimic the mechanical properties of a broad range of biological tissues [141].

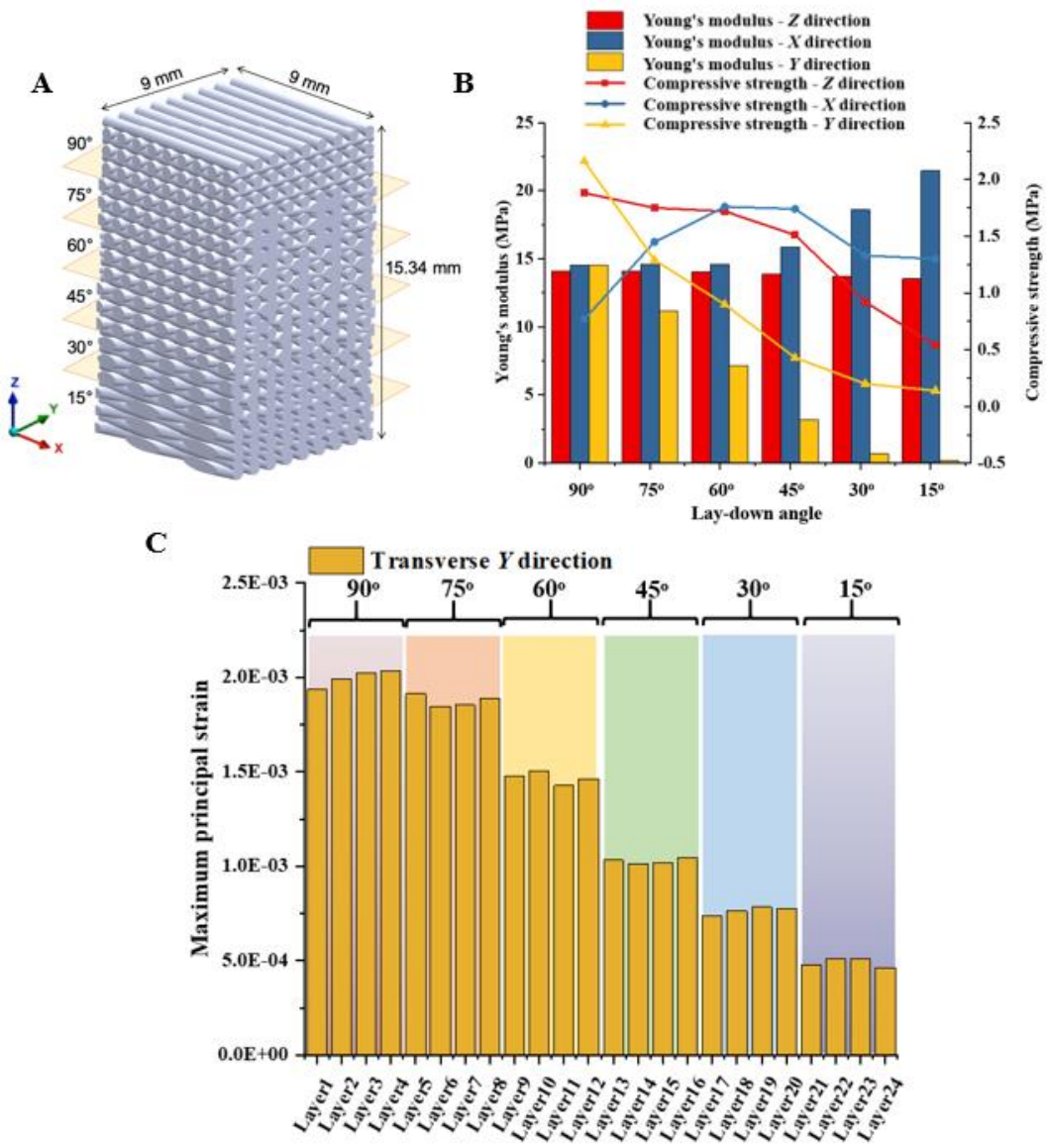

Figure 7. (A) A complex scaffold structure assembled by six sections with different lay down angles in a single construct. (B) Young's modulus and compressive strength values of cubic scaffolds with different lay down angles compressed in three orthogonal directions. (C) Plots of maximum principal strains of filament surfaces compressed in the *Y* direction gradient decrease within the complex assembled scaffold structure [80]. Reprinted from ref. 80 with permission from Elsevier, Copyright 2020.

The application of FE modeling for the analysis of scaffold mechanical properties under perfusion fluid dynamic environment has been evaluated; Olivares *et al.* proposed various scaffold structures, including gyroid and hexagonal scaffolds with 55% and 70% porosity as well as gyroid scaffolds with porosity gradient at longitudinal and radial directions. They studied the effect of fluid shear stress distribution on the scaffolds under an inlet fluid flow velocity at 0.1 mm/s using the FE method. The simulation results were analyzed using the mechano-regulation theory. The results indicated that the distribution of shear stress induced by fluid perfusion was dependent on the pore distribution within the scaffold. The differentiation process in these scaffold structures was more sensitive to the inlet fluid flow than the compressive strain [142]. Other studies applied FE modeling and *in vitro* experiments together to investigate the fluid shear stress generated on scaffolds for MSCs differentiation. Melchels *et al.* simulated the fluid shear stress within uniform gyroid scaffolds in a perfusing fluid; they compared the simulation results with the *in vitro* experimental results. They fabricated a photo-polymerizable poly-D, L-lactic acid scaffold with 62% porosity using 3D printing and seeded the scaffold with human articular chondrocytes. The results revealed that the highest cell density was in the region of the scaffold where the wall shear stress of the fluid flow was the highest (3.8×10^{-3} Pa) [115]. Grayson *et al.* modeled the flow patterns to determine the relationship between interstitial flow and tissue development. A comparison of mathematical modeling results with *in vitro* experimental data indicated that the density and architecture of the bone matrix were related to the intensity and pattern of the interstitial flow [143]. Xue *et al.* developed a dual-chamber perfusion bioreactor system that cocultured ATDC5 and MC3T3-E1 cells on a 3D printed scaffold (Figure 8 A). A FE method that evaluated the CAD and microcomputed tomography images of the manufactured scaffold was utilized; the microenvironment inside the two FE models was studied (Figure 8 B). *In vitro* results showed that the co-culture system supported OC tissue growth in terms of cell viability, proliferation,

distribution, and attachment (Figure 8 C). The FE simulation results showed that the CAD and the actual manufactured scaffold had significant differences in the flow velocity, differentiation medium mixing in the bioreactor, and fluid-induced shear stress experienced by the cells. This system was shown to have the desired microenvironment for OC tissue engineering; this approach can potentially be used as an inexpensive tool for testing newly developed tissue scaffolds [33].

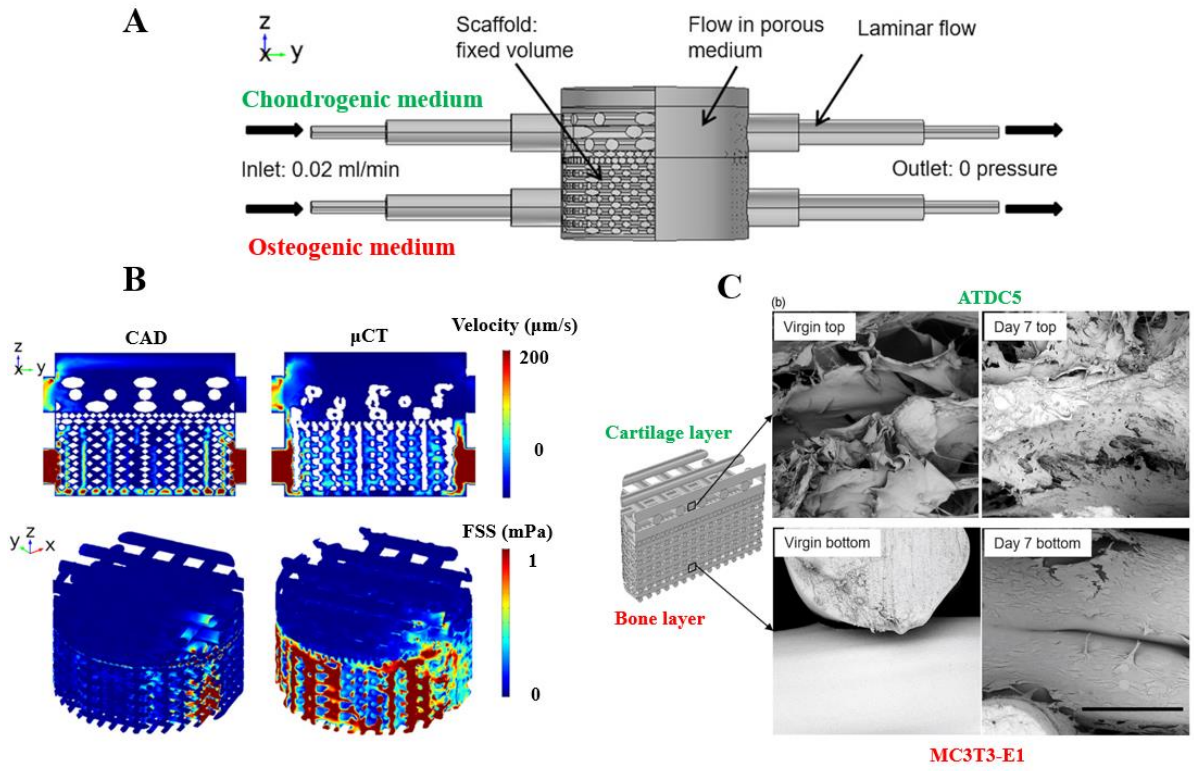

Figure 8. (A) CAD model of perfusion coculture and boundary conditions used in the FE model. (B) Flow velocity and fluid induced shear stress distribution for CAD and µCT model. (C) SEM micrographs of the top (containing ATDC5 cells) and bottom (containing MC3T3-E1 cells) layers in the virgin scaffold and the cell-containing scaffold at Day 7; scale bar = 300 µm [33]. Reprinted from ref. 33 with permission from John Wiley and Sons, Copyright 2019.

4.6 Commercial gradient OC scaffolds in clinical trials

To this point, very few scaffold designs have been evaluated using clinical trials. Commercially available tissue scaffolds for OC regeneration are mainly biphasic or triphasic scaffolds that

mimic the entire OC unit, (Figure 9). For instance, the TruFit plug from Smith & Nephew is a classic biphasic scaffold consisting of porous PLGA/PGA and calcium phosphate. Although the clinical findings of TruFit plug did demonstrate stable cartilage-like repair over a short term (less than one year), the long-term results (more than two years) were questionable; this result is attributed to delayed and inadequate integration with the surrounding tissue [144,145]. Dell'Osso *et al*. indicated that the scaffold would exhibit better performance if the design more closely mimicked the surrounding OC tissue rather than the biphasic approach [146].

One recently developed scaffold that is undergoing clinical trials is the triphasic MaioRegen from Fin-Ceramica Faenza SpA; this scaffold attempts to more closely mimic the structure of OC tissue. The cartilage layer consists of equine type I collagen; the calcified cartilage layer consists of type I collagen (60% of total weight) and magnesium-hydroxyapatite (Mg-HAp) (40% of total weight). The bone layer consists of a mineralized blend of type I collagen (30% of weight) and Mg-HAp (70% of weight). A clinical study by Kon *et al.* indicated that subchondral bone formation occurred, with complete resorption of the biomaterial. The cartilage tissue was not only repaired but also participated in an ongoing maturation process over six months [147]. They performed an analysis five years post-surgery with the MaioRegen treatment and MRI evaluation and demonstrated revealed significant improvement in both cartilage and subchondral bone [148]. However, a recent study by Christensen *et al.* observed opposite and adverse outcomes; incomplete cartilage repair and poor subchondral bone repair after ankle and knee joint treatments with the MaioRegen scaffold were noted [149]. Thus, the available commercial products indicate the advantages of a gradient structure that closely mimics the natural structure of the OC tissue, however, significant efforts still need to be performed to significantly increase the regenerative capacity of OC replacements [149-151].

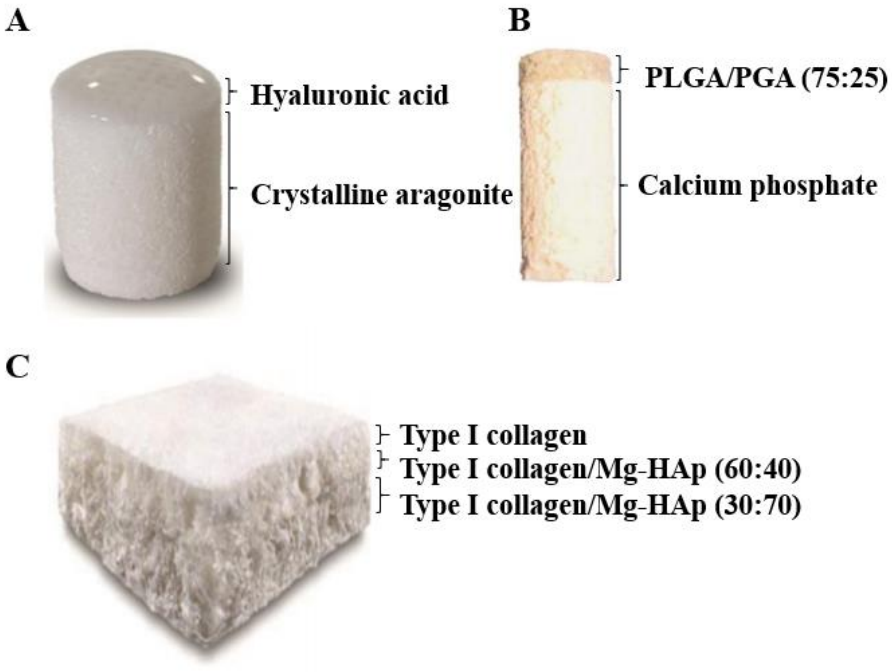

Figure 9. Images of gradient scaffolds that reached clinical trials. (A) Crystalline aragonite based biphasic scaffold (Agili-C, CartiHeal, Israel). (B) Polymeric PLGA/PGA and Calcium sulfate biphasic scaffold (Trufit, Smith & Nephew, USA). (C) Collagen type I and HAp triphasic scaffold (MaioRegen, Finceramica, Italy) [145]. Reprinted from ref. 145 with permission from Molecular Diversity Preservation International, Copyright 2019.

5 Challenges and future perspectives

This review summarizes the gradient characteristics of OC tissue from the superficial zone of cartilage to the subchondral bone in terms of biochemical composition, structure, and mechanical properties. The application of tissue engineering and the development of tissue scaffolds to mimic gradient factors for OC repair are discussed. Although most *in vitro* and *in vivo* studies yield good results for OC tissue regeneration, longer-term clinical studies did not provide satisfactory results; further studies into tissue scaffolds for OC regeneration are still required. The laboratory studies indicate that a continuous gradient scaffold is more promising than a discrete gradient scaffold since it can mimic the OC tissue structure without the abrupt changes between layers; studies of continuous gradient scaffolds for OC repair are currently underway.

Conventional fabrication methods such as solvent-casting, gas forming, freeze-drying, and electrospinning have been used to fabricate OC tissue scaffolds due to the compatibility of these methods with a wide range of materials, control over scaffold pore size, control over porosity, and low cost. Various 3D printing methods such as solid, powder and liquid-based methods have been used for OC tissue scaffold processing since they provide a high degree of control over pore geometry and enable processing of highly interconnected pore structures. One of the limitations associated with the use of 3D printing for OC tissue regeneration is the absence of appropriate materials for processing of OC scaffolds. New synthetic or composite materials with non-toxic, biodegradable, chondrogenic, and osteogenic characteristics are required to produce OC tissue. Although 3D printing can be used to create scaffolds based on CAD designs, studies indicate that there are significant differences between the microcomputed tomography image of the manufactured scaffold and the CAD model. Those differences may be associated with the 3D printing process; thus, the optimization of the 3D printing process for scaffold fabrication is needed.

Scaffold-bioreactor systems are capable of providing appropriate stimuli to guide tissue differentiation and generation for OC repair. The OC scaffolds can be placed into an anatomically shaped bioreactor chamber to stimulate tissue regeneration. However, the relationship among cells, scaffolds, and mechanical stimuli are blurred; studies are needed to examine the influence of the materials, scaffold structure, and bioreactor systems for tissue regeneration. In particular, most studies indicate that scaffold pore size and porosity can affect osteogenesis and chondrogenesis; however, there are few studies that examine the influence of pore shape on tissue generation for OC repair. Since the collagen fibers within OC tissue have different orientations, an investigation of the relationship between tissue regeneration and

filament orientation within 3D scaffolds may facilitate the development of an ideal gradient scaffold for OC tissue repair.

Furthermore, the combination of FE simulation and 3D printing brings an important perspective to OC tissue scaffold development. The assessment of 3D printed scaffold models that are generated from microcomputed tomography images in terms of the compressive strain and fluid wall shear stress, both under compressive loading and in a fluid dynamic environment, using the FE modeling approach is a low-cost and efficient method for OC tissue scaffold development.

Disclosure statement

There is no potential conflict of interest in this work.

References

(1) *OARSI White Paper- OA as a Serious Disease;* Administration, F. a. D., World Health Organization, 2016.

(2) Chiang, H.; Jiang, C.-C. Repair of articular cartilage defects: review and perspectives. *Journal of the Formosan Medical Association* **2009**, *108*, 87-101.

(3) Tibor, L. M.; Weiss, J. A. Hip cartilage restoration: Overview. *Hip Arthroscopy and Hip Joint Preservation Surgery* **2013**, 1-19.

(4) Gill, T. J.; Asnis, P. D.; Berkson, E. M. The treatment of articular cartilage defects using the microfracture technique. *Journal of Orthopaedic & Sports Physical Therapy* **2006**, *36*, 728-738.

(5) Vacanti, J. P.; Langer, R. Tissue engineering: the design and fabrication of living replacement devices for surgical reconstruction and transplantation. *The lancet* **1999**, *354*, S32-S34.

(6) Bauer, T. W.; Muschler, G. F. Bone graft materials: an overview of the basic science. *Clinical Orthopaedics and Related Research®* **2000**, *371*, 10-27.

(7) Miron RJ, S. A., Shuang Y, Bosshardt DD, Gruber R, Buser D, Chandad F, Zhang Y. Osteoinductive potential of a novel biphasic calcium phosphate bone graft in comparison with autographs, xenografts, and DFDBA. *Clinical Oral Implants* **2015**.

(8) Bittner, S. M.; Smith, B. T.; Diaz-Gomez, L.; Hudgins, C. D.; Melchiorri, A. J.; Scott, D. W.; Fisher, J. P.; Mikos, A. G. Fabrication and mechanical characterization of 3D printed vertical uniform and gradient scaffolds for bone and osteochondral tissue engineering. *Acta biomaterialia* **2019**, *90*, 37-48.

(9) Chen, L.; Deng, C.; Li, J.; Yao, Q.; Chang, J.; Wang, L.; Wu, C. 3D printing of a lithium-calcium-silicate crystal bioscaffold with dual bioactivities for osteochondral interface reconstruction. *Biomaterials* **2019**, *196*, 138-150.

(10) Kosik-Kozioł, A.; Heljak, M.; Święszkowski, W. Mechanical Properties of Hybrid Triphasic Scaffolds for Osteochondral Tissue Engineering. *Materials Letters* **2019**, 126893.

(11) Nowicki, M.; Zhu, W.; Sarkar, K.; Rao, R.; Zhang, L. G. 3D Printing Multiphasic Osteochondral Tissue Constructs with Nano to Micro Features via PCL based Bioink. *Bioprinting* **2019**, e00066.

(12) Li, Z.; Jia, S.; Xiong, Z.; Long, Q.; Yan, S.; Hao, F.; Liu, J.; Yuan, Z. 3D-printed scaffolds with calcified layer for osteochondral tissue engineering. *Journal of bioscience and bioengineering* **2018**, *126*, 389-396.

(13) Zhou, X.; Esworthy, T.; Lee, S.-J.; Miao, S.; Cui, H.; Plesiniak, M.; Fenniri, H.; Webster, T.; Rao, R. D.; Zhang, L. G. 3D Printed scaffolds with hierarchical biomimetic structure for osteochondral regeneration. *Nanomedicine: Nanotechnology, Biology and Medicine* **2019**, *19*, 58-70.

(14) Kang, H.; Zeng, Y.; Varghese, S. Functionally graded multilayer scaffolds for in vivo osteochondral tissue engineering. *Acta biomaterialia* **2018**, *78*, 365-377.

(15) Ansari, S.; Khorshidi, S.; Karkhaneh, A. Engineering of gradient osteochondral tissue: From nature to lab. *Acta biomaterialia* **2019**.

(16) Mohan, N.; Dormer, N. H.; Caldwell, K. L.; Key, V. H.; Berkland, C. J.; Detamore, M. S. Continuous gradients of material composition and growth factors for effective regeneration of the osteochondral interface. *Tissue Engineering Part A* **2011**, *17*, 2845-2855.

(17) Dormer, N. H.; Singh, M.; Wang, L.; Berkland, C. J.; Detamore, M. S. Osteochondral interface tissue engineering using macroscopic gradients of bioactive signals. *Annals of biomedical engineering* **2010**, *38*, 2167-2182.

(18) Nooeaid, P.; Salih, V.; Beier, J. P.; Boccaccini, A. R. Osteochondral tissue engineering: scaffolds, stem cells and applications. *Journal of cellular and molecular medicine* **2012**, *16*, 2247-2270.

(19) Schaefer, D.; Martin, I.; Shastri, P.; Padera, R.; Langer, R.; Freed, L.; Vunjak-Novakovic, G. In vitro generation of osteochondral composites. *Biomaterials* **2000**, *21*, 2599-2606.

(20) Eltom, A.; Zhong, G.; Muhammad, A. Scaffold techniques and designs in tissue engineering functions and purposes: a review. *Advances in Materials Science and Engineering* **2019**, *2019*.

(21) Lee, P.; Manoukian, O. S.; Zhou, G.; Wang, Y.; Chang, W.; Yu, X.; Kumbar, S. G. Osteochondral scaffold combined with aligned nanofibrous scaffolds for cartilage regeneration. *RSC advances* **2016**, *6*, 72246-72255.

(22) Loh, Q. L.; Choong, C. Three-dimensional scaffolds for tissue engineering applications: role of porosity and pore size. *Tissue Engineering Part B: Reviews* **2013**, *19*, 485-502.

(23) Hutmacher, D. W.: Scaffolds in tissue engineering bone and cartilage. In *The Biomaterials: Silver Jubilee Compendium*; Elsevier, 2006; pp 175-189.

(24) Levingstone, T. J.; Matsiko, A.; Dickson, G. R.; O'Brien, F. J.; Gleeson, J. P. A biomimetic multi-layered collagen-based scaffold for osteochondral repair. *Acta biomaterialia* **2014**, *10*, 1996-2004.

(25) Shi, D.; Shen, J.; Zhang, Z.; Shi, C.; Chen, M.; Gu, Y.; Liu, Y. Preparation and properties of dopamine‐modified alginate/chitosan–hydroxyapatite scaffolds with gradient structure for bone tissue engineering. *Journal of Biomedical Materials Research Part A* **2019**, *107*, 1615-1627.

(26) Korpayev, S.; Kaygusuz, G.; Şen, M.; Orhan, K.; Oto, Ç.; Karakeçili, A. Chıtosan/collagen based biomimetic osteochondral tissue constructs: A growth factor-free approach. *International Journal of Biological Macromolecules* **2020**.

(27) Parisi, C.; Salvatore, L.; Veschini, L.; Serra, M. P.; Hobbs, C.; Madaghiele, M.; Sannino, A.; Di Silvio, L. Biomimetic gradient scaffold of collagen–hydroxyapatite for osteochondral regeneration. *Journal of Tissue Engineering* **2020**, *11*, 2041731419896068.

(28) Zhang, S.; Chen, L.; Jiang, Y.; Cai, Y.; Xu, G.; Tong, T.; Zhang, W.; Wang, L.; Ji, J.; Shi, P. Bi-layer collagen/microporous electrospun nanofiber scaffold improves the osteochondral regeneration. *Acta Biomaterialia* **2013**, *9*, 7236-7247.

(29) McCullen, S. D.; Miller, P. R.; Gittard, S. D.; Gorga, R. E.; Pourdeyhimi, B.; Narayan, R. J.; Loboa, E. G. In situ collagen polymerization of layered cell-seeded electrospun scaffolds for bone tissue engineering applications. *Tissue Engineering Part C: Methods* **2010**, *16*, 1095-1105.

(30) Rebollar, E.; Cordero, D.; Martins, A.; Chiussi, S.; Reis, R. L.; Neves, N. M.; León, B. Improvement of electrospun polymer fiber meshes pore size by femtosecond laser irradiation. *Applied Surface Science* **2011**, *257*, 4091-4095.

(31) Lin, H.; Lozito, T. P.; Alexander, P. G.; Gottardi, R.; Tuan, R. S. Stem cell-based microphysiological osteochondral system to model tissue response to interleukin-1β. *Molecular pharmaceutics* **2014**, *11*, 2203-2212.

(32) Hung, C. T.; Mauck, R. L.; Wang, C. C.-B.; Lima, E. G.; Ateshian, G. A. A paradigm for functional tissue engineering of articular cartilage via applied physiologic deformational loading. *Annals of biomedical engineering* **2004**, *32*, 35-49.

(33) Xue, R.; Chung, B.; Tamaddon, M.; Carr, J.; Liu, C.; Cartmell, S. H. Osteochondral tissue coculture: An in vitro and in silico approach. *Biotechnology and bioengineering* **2019**, *116*, 3112-3123.

(34) Di Luca, A.; Van Blitterswijk, C.; Moroni, L. The osteochondral interface as a gradient tissue: From development to the fabrication of gradient scaffolds for regenerative medicine. *Birth Defects Research Part C: Embryo Today: Reviews* **2015**, *105*, 34-52.

(35) Martin, I.; Miot, S.; Barbero, A.; Jakob, M.; Wendt, D. Osteochondral tissue engineering. *Journal of biomechanics* **2007**, *40*, 750-765.

(36) Sophia Fox, A. J.; Bedi, A.; Rodeo, S. A. The basic science of articular cartilage: structure, composition, and function. *Sports health* **2009**, *1*, 461-468.

(37) Zhang, L.; Hu, J.; Athanasiou, K. A. The role of tissue engineering in articular cartilage repair and regeneration. *Critical Reviews™ in Biomedical Engineering* **2009**, *37*.

(38) Panadero, J.; Lanceros-Mendez, S.; Ribelles, J. G. Differentiation of mesenchymal stem cells for cartilage tissue engineering: individual and synergetic effects of three-dimensional environment and mechanical loading. *Acta biomaterialia* **2016**, *33*, 1-12.

(39) Gong, T.; Xie, J.; Liao, J.; Zhang, T.; Lin, S.; Lin, Y. Nanomaterials and bone regeneration. *Bone research* **2015**, *3*, 15029.

(40) Betts, J.; DeSaix, P.; Johnson, E.; Johnson, J.; Korol, O.: Anatomy and Physiology. Houston, TX: OpenStax College. 2013.

(41) Comper, W. D.: *Extracellular matrix*; Crc Press, 1996; Vol. 1.

(42) Antons, J.; Marascio, M. G. M.; Nohava, J.; Martin, R.; Applegate, L.; Bourban, P.; Pioletti, D. Zone-dependent mechanical properties of human articular cartilage obtained by indentation measurements. *Journal of Materials Science: Materials in Medicine* **2018**, *29*, 57.

(43) Khanarian, N. T.; Haney, N. M.; Burga, R. A.; Lu, H. H. A functional agarose-hydroxyapatite scaffold for osteochondral interface regeneration. *Biomaterials* **2012**, *33*, 5247-5258.

(44) Zhang, B.; Guo, L.; Chen, H.; Ventikos, Y.; Narayan, R. J.; Huang, J. Finite element evaluations of the mechanical properties of polycaprolactone/hydroxyapatite scaffolds

by direct ink writing: Effects of pore geometry. *Journal of the Mechanical Behavior of Biomedical Materials* **2020**, 103665.

(45) Steele, J.; McCullen, S.; Callanan, A.; Autefage, H.; Accardi, M.; Dini, D.; Stevens, M. Combinatorial scaffold morphologies for zonal articular cartilage engineering. *Acta biomaterialia* **2014**, *10*, 2065-2075.

(46) Zhang, B.; Huang, J.; Narayan, R.: Nanostructured biomaterials for regenerative medicine: Clinical perspectives. In *Nanostructured Biomaterials for Regenerative Medicine*; Elsevier, 2020; pp 47-80.

(47) Tripathy, N.; Perumal, E.; Ahmad, R.; Song, J. E.; Khang, G.: Hybrid composite biomaterials. In *Principles of Regenerative Medicine*; Elsevier, 2019; pp 695-714.

(48) Lee, S.; Porter, M.; Wasko, S.; Lau, G.; Chen, P.-Y.; Novitskaya, E. E.; Tomsia, A. P.; Almutairi, A.; Meyers, M. A.; McKittrick, J. Potential bone replacement materials prepared by two methods. *MRS Online Proceedings Library Archive* **2012**, *1418*.

(49) Zhang, Y.; Wang, F.; Tan, H.; Chen, G.; Guo, L.; Yang, L. Analysis of the mineral composition of the human calcified cartilage zone. *International journal of medical sciences* **2012**, *9*, 353.

(50) Molino, G.; Palmieri, M. C.; Montalbano, G.; Fiorilli, S.; Vitale-Brovarone, C. Biomimetic and mesoporous nano-hydroxyapatite for bone tissue application: a short review. *Biomedical Materials* **2020**, *15*, 022001.

(51) Li, G.; Yin, J.; Gao, J.; Cheng, T. S.; Pavlos, N. J.; Zhang, C.; Zheng, M. H. Subchondral bone in osteoarthritis: insight into risk factors and microstructural changes. *Arthritis research & therapy* **2013**, *15*, 223.

(52) Ng, H. Y.; Lee, K.-X. A.; Shen, Y.-F. Articular cartilage: structure, composition, injuries and repair. *JSM Bone and Joint Dis* **2017**, *1*, 1010.

(53) Kalia, P.; Vizcay-Barrena, G.; Fan, J. P.; Warley, A.; Di Silvio, L.; Huang, J. Nanohydroxyapatite shape and its potential role in bone formation: an analytical study. *Journal of The Royal Society Interface* **2014**, *11*, 20140004.

(54) Nikolov, S.; Raabe, D. Hierarchical modeling of the elastic properties of bone at submicron scales: the role of extrafibrillar mineralization. *Biophysical journal* **2008**, *94*, 4220-4232.

(55) Hadjidakis, D. J.; Androulakis, I. I. Bone remodeling. *Annals of the New York Academy of Sciences* **2006**, *1092*, 385-396.

(56) Sabree, I.; Gough, J.; Derby, B. Mechanical properties of porous ceramic scaffolds: influence of internal dimensions. *Ceramics International* **2015**, *41*, 8425-8432.

(57) Boschetti, F.; Pennati, G.; Gervaso, F.; Peretti, G. M.; Dubini, G. Biomechanical properties of human articular cartilage under compressive loads. *Biorheology* **2004**, *41*, 159-166.

(58) Walther, A.; Hoyer, B.; Springer, A.; Mrozik, B.; Hanke, T.; Cherif, C.; Pompe, W.; Gelinsky, M. Novel textile scaffolds generated by flock technology for tissue engineering of bone and cartilage. *Materials* **2012**, *5*, 540-557.

(59) Gao, L.-L.; Zhang, C.-Q.; Gao, H.; Liu, Z.-D.; Xiao, P.-P. Depth and rate dependent mechanical behaviors for articular cartilage: experiments and theoretical predictions. *Materials Science and Engineering: C* **2014**, *38*, 244-251.

(60) Qu, H.; Fu, H.; Han, Z.; Sun, Y. Biomaterials for bone tissue engineering scaffolds: a review. *RSC advances* **2019**, *9*, 26252-26262.

(61) Athanasiou, K.; Agarwal, A.; Dzida, F. Comparative study of the intrinsic mechanical properties of the human acetabular and femoral head cartilage. *Journal of Orthopaedic Research* **1994**, *12*, 340-349.

(62) Gibson, L. J. The mechanical behaviour of cancellous bone. *Journal of biomechanics* **1985**, *18*, 317-328.

(63) Helguero, C. G.; Mustahsan, V. M.; Parmar, S.; Pentyala, S.; Pfail, J. L.; Kao, I.; Komatsu, D. E.; Pentyala, S. Biomechanical properties of 3D-printed bone scaffolds are improved by treatment with CRFP. *Journal of orthopaedic surgery and research* **2017**, *12*, 195.

(64) Heinegård, D.; Saxne, T. The role of the cartilage matrix in osteoarthritis. *Nature Reviews Rheumatology* **2011**, *7*, 50.

(65) Jones, D. G.; Peterson, L. Autologous chondrocyte implantation. *JBJS* **2006**, *88*, 2501-2520.

(66) Minas, T. Autologous chondrocyte implantation for focal chondral defects of the knee. *Clinical Orthopaedics and Related Research®* **2001**, *391*, S349-S361.

(67) Control, C. f. D. Transmission of HIV through bone transplantation: case report and public health recommendations. *MMWR. Morbidity and mortality weekly report* **1988**, *37*, 597.

(68) Bauer, T. W.; Schils, J. The pathology of total joint arthroplasty. I. Mechanisms of implant fixation. *Skeletal radiology* **1999**, *28*, 423-432.

(69) Williams, G. M.; Chan, E. F.; Temple-Wong, M. M.; Bae, W. C.; Masuda, K.; Bugbee, W. D.; Sah, R. L. Shape, loading, and motion in the bioengineering design, fabrication, and testing of personalized synovial joints. *Journal of biomechanics* **2010**, *43*, 156-165.

(70) Yousefi, A. M.; Hoque, M. E.; Prasad, R. G.; Uth, N. Current strategies in multiphasic scaffold design for osteochondral tissue engineering: a review. *Journal of biomedical materials research Part A* **2015**, *103*, 2460-2481.

(71) Gadjanski, I. Mimetic Hierarchical Approaches for Osteochondral Tissue Engineering. *Osteochondral Tissue Engineering: Nanotechnology, Scaffolding-Related Developments and Translation* **2018**, 143-170.

(72) Han, Y.; Li, X.; Zhang, Y.; Han, Y.; Chang, F.; Ding, J. Mesenchymal stem cells for regenerative medicine. *Cells* **2019**, *8*, 886.

(73) Du, M.; Chen, B.; Meng, Q.; Liu, S.; Zheng, X.; Zhang, C.; Wang, H.; Li, H.; Wang, N.; Dai, J. 3D bioprinting of BMSC-laden methacrylamide gelatin scaffolds with CBD-BMP2-collagen microfibers. *Biofabrication* **2015**, *7*, 044104.

(74) Trachtenberg, J. E.; Placone, J. K.; Smith, B. T.; Fisher, J. P.; Mikos, A. G. Extrusion-based 3D printing of poly (propylene fumarate) scaffolds with hydroxyapatite gradients. *Journal of Biomaterials Science, Polymer Edition* **2017**, *28*, 532-554.

(75) Gao, F.; Xu, Z.; Liang, Q.; Liu, B.; Li, H.; Wu, Y.; Zhang, Y.; Lin, Z.; Wu, M.; Ruan, C. Direct 3D printing of high strength biohybrid gradient hydrogel scaffolds for efficient repair of osteochondral defect. *Advanced Functional Materials* **2018**, *28*, 1706644.

(76) Stratton, S.; Shelke, N. B.; Hoshino, K.; Rudraiah, S.; Kumbar, S. G. Bioactive polymeric scaffolds for tissue engineering. *Bioactive materials* **2016**, *1*, 93-108.

(77) Dash, M.; Chiellini, F.; Ottenbrite, R. M.; Chiellini, E. Chitosan—A versatile semi-synthetic polymer in biomedical applications. *Progress in polymer science* **2011**, *36*, 981-1014.

(78) S. Van Bael , Y. C. C., S. Truscello, M. Moesen, G. Kerckhofs, H. Van Oosterwyck, J.-P. Kruth, J. Schrooten. The effect of pore geometry on the in vitro biological behavior of human periosteum-derived cells seeded on selective laser-melted Ti6Al4V bone scaffolds. *Acta Biomaterialia* **2012**, *8*, 2824–2834.

(79) Nowicki, M. A.; Castro, N. J.; Plesniak, M. W.; Zhang, L. G. 3D printing of novel osteochondral scaffolds with graded microstructure. *Nanotechnology* **2016**, *27*, 414001.

(80) Zhang, B.; Guo, L.; Chen, H.; Ventikos, Y.; Narayan, R. J.; Huang, J. Finite element evaluations of the mechanical properties of polycaprolactone/hydroxyapatite scaffolds by direct ink writing: Effects of pore geometry. *Journal of the Mechanical Behavior of Biomedical Materials* **2020**, *104*, 103665.

(81) Grayson, W. L.; Bhumiratana, S.; Chao, P. G.; Hung, C. T.; Vunjak-Novakovic, G. Spatial regulation of human mesenchymal stem cell differentiation in engineered osteochondral constructs: effects of pre-differentiation, soluble factors and medium perfusion. *Osteoarthritis and cartilage* **2010**, *18*, 714-723.

(82) Byers, B. A.; Mauck, R. L.; Chiang, I. E.; Tuan, R. S. Transient exposure to transforming growth factor beta 3 under serum-free conditions enhances the biomechanical and biochemical maturation of tissue-engineered cartilage. *Tissue Engineering Part A* **2008**, *14*, 1821-1834.

(83) Buxton, A. N.; Bahney, C. S.; Yoo, J. U.; Johnstone, B. Temporal exposure to chondrogenic factors modulates human mesenchymal stem cell chondrogenesis in hydrogels. *Tissue Engineering Part A* **2011**, *17*, 371-380.

(84) Abrahamsson, C. K.; Yang, F.; Park, H.; Brunger, J. M.; Valonen, P. K.; Langer, R.; Welter, J. F.; Caplan, A. I.; Guilak, F.; Freed, L. E. Chondrogenesis and mineralization during in vitro culture of human mesenchymal stem cells on three-dimensional woven scaffolds. *Tissue Engineering Part A* **2010**, *16*, 3709-3718.

(85) Loozen, L. D.; Wegman, F.; Öner, F. C.; Dhert, W. J.; Alblas, J. Porous bioprinted constructs in BMP-2 non-viral gene therapy for bone tissue engineering. *Journal of Materials Chemistry B* **2013**, *1*, 6619-6626.

(86) Liao, C.-T.; Ho, M.-H. The fabrication of biomimetic chitosan scaffolds by using SBF treatment with different crosslinking agents. *Membranes* **2011**, *1*, 3-12.

(87) Abarrategi, A.; López-Morales, Y.; Ramos, V.; Civantos, A.; López-Durán, L.; Marco, F.; López-Lacomba, J. L. Chitosan scaffolds for osteochondral tissue regeneration. *Journal of Biomedical Materials Research Part A* **2010**, *95*, 1132-1141.

(88) Zanetti, A. S.; Sabliov, C.; Gimble, J. M.; Hayes, D. J. Human adipose-derived stem cells and three-dimensional scaffold constructs: A review of the biomaterials and models currently used for bone regeneration. *Journal of Biomedical Materials Research Part B: Applied Biomaterials* **2013**, *101*, 187-199.

(89) Zhou, J.; Xu, C.; Wu, G.; Cao, X.; Zhang, L.; Zhai, Z.; Zheng, Z.; Chen, X.; Wang, Y. In vitro generation of osteochondral differentiation of human marrow mesenchymal stem cells in novel collagen–hydroxyapatite layered scaffolds. *Acta biomaterialia* **2011**, *7*, 3999-4006.

(90) Wang, Y.; Blasioli, D. J.; Kim, H.-J.; Kim, H. S.; Kaplan, D. L. Cartilage tissue engineering with silk scaffolds and human articular chondrocytes. *Biomaterials* **2006**, *27*, 4434-4442.

(91) Gervaso, F.; Sannino, A.; Peretti, G. M. The biomaterialist's task: scaffold biomaterials and fabrication technologies. *Joints* **2013**, *1*, 130-137.

(92) Rezwan, K.; Chen, Q.; Blaker, J.; Boccaccini, A. R. Biodegradable and bioactive porous polymer/inorganic composite scaffolds for bone tissue engineering. *Biomaterials* **2006**, *27*, 3413-3431.

(93) Baker, B. M.; Shah, R. P.; Silverstein, A. M.; Esterhai, J. L.; Burdick, J. A.; Mauck, R. L. Sacrificial nanofibrous composites provide instruction without impediment and enable functional tissue formation. *Proceedings of the National Academy of Sciences* **2012**, *109*, 14176-14181.

(94) Park, S. A.; Lee, S. J.; Seok, J. M.; Lee, J. H.; Kim, W. D.; Kwon, I. K. Fabrication of 3D Printed PCL/PEG Polyblend Scaffold Using Rapid Prototyping System for Bone Tissue Engineering Application. *Journal of Bionic Engineering* **2018**, *15*, 435-442.

(95) Hench, L. L. The story of Bioglass®. *Journal of Materials Science: Materials in Medicine* **2006**, *17*, 967-978.

(96) Liu, J.; Li, L.; Suo, H.; Yan, M.; Yin, J.; Fu, J. 3D printing of biomimetic multi-layered GelMA/nHA scaffold for osteochondral defect repair. *Materials & Design* **2019**, *171*, 107708.

(97) Chen, J.; Chen, H.; Li, P.; Diao, H.; Zhu, S.; Dong, L.; Wang, R.; Guo, T.; Zhao, J.; Zhang, J. Simultaneous regeneration of articular cartilage and subchondral bone in vivo using MSCs induced by a spatially controlled gene delivery system in bilayered integrated scaffolds. *Biomaterials* **2011**, *32*, 4793-4805.

(98) Zhao, C.; Zhang, H.; Cai, B.; Wang, G.; Fan, H.; Zhang, X. Preparation of porous PLGA/Ti biphasic scaffold and osteochondral defect repair. *Biomaterials Science* **2013**, *1*, 703-710.

(99) Jiang, J.; Tang, A.; Ateshian, G. A.; Guo, X. E.; Hung, C. T.; Lu, H. H. Bioactive stratified polymer ceramic-hydrogel scaffold for integrative osteochondral repair. *Annals of biomedical engineering* **2010**, *38*, 2183-2196.

(100) Nooeaid, P.; Roether, J. A.; Weber, E.; Schubert, D. W.; Boccaccini, A. R. Technologies for multilayered scaffolds suitable for interface tissue engineering. *Advanced Engineering Materials* **2014**, *16*, 319-327.

(101) La Carrubba, V.; Pavia, F. C.; De Luca, A.; Giavaresi, G. In *Tilte*2018; IEEE.

(102) Liu, W.; Zhang, Y. S.; Heinrich, M. A.; De Ferrari, F.; Jang, H. L.; Bakht, S. M.; Alvarez, M. M.; Yang, J.; Li, Y. C.; Trujillo‐de Santiago, G. Rapid continuous multimaterial extrusion bioprinting. *Advanced materials* **2017**, *29*, 1604630.

(103) Karageorgiou, V.; Kaplan, D. Porosity of 3D biomaterial scaffolds and osteogenesis. *Biomaterials* **2005**, *26*, 5474-5491.

(104) Kim, K.; Yeatts, A.; Dean, D.; Fisher, J. P. Stereolithographic bone scaffold design parameters: osteogenic differentiation and signal expression. *Tissue Engineering Part B: Reviews* **2010**, *16*, 523-539.

(105) Marrella, A.; Lee, T. Y.; Lee, D. H.; Karuthedom, S.; Syla, D.; Chawla, A.; Khademhosseini, A.; Jang, H. L. Engineering vascularized and innervated bone biomaterials for improved skeletal tissue regeneration. *Materials Today* **2018**, *21*, 362-376.

(106) Wang, Y.; Meng, H.; Yuan, X.; Peng, J.; Guo, Q.; Lu, S.; Wang, A. Fabrication and in vitro evaluation of an articular cartilage extracellular matrix-hydroxyapatite bilayered scaffold with low permeability for interface tissue engineering. *Biomedical engineering online* **2014**, *13*, 80.

(107) Xiao, H.; Huang, W.; Xiong, K.; Ruan, S.; Yuan, C.; Mo, G.; Tian, R.; Zhou, S.; She, R.; Ye, P. Osteochondral repair using scaffolds with gradient pore sizes constructed with silk fibroin, chitosan, and nano-hydroxyapatite. *International journal of nanomedicine* **2019**, *14*, 2011.

(108) Choi, S.-W.; Zhang, Y.; Xia, Y. Three-dimensional scaffolds for tissue engineering: the importance of uniformity in pore size and structure. *Langmuir* **2010**, *26*, 19001-19006.

(109) Engler, A. J.; Sen, S.; Sweeney, H. L.; Discher, D. E. Matrix Elasticity Directs Stem Cell Lineage Specification. *Cell* **2006**, *126*, 677-689.

(110) Lin, T.-H.; Wang, H.-C.; Cheng, W.-H.; Hsu, H.-C.; Yeh, M.-L. Osteochondral tissue regeneration using a tyramine-modified bilayered PLGA scaffold combined with articular chondrocytes in a porcine model. *International journal of molecular sciences* **2019**, *20*, 326.

(111) Giannoni, P.; Lazzarini, E.; Ceseracciu, L.; Barone, A. C.; Quarto, R.; Scaglione, S. Design and characterization of a tissue‐engineered bilayer scaffold for osteochondral tissue repair. *Journal of tissue engineering and regenerative medicine* **2015**, *9*, 1182-1192.

(112) Gloria, A.; Russo, T.; De Santis, R.; Ambrosio, L. 3D fiber deposition technique to make multifunctional and tailor-made scaffolds for tissue engineering applications. *Journal of Applied Biomaterials and Biomechanics* **2009**, *7*, 141-152.

(113) Andrea Di Luca, B., Ivan Lorenzo-Moldero, Antonio Lepedda, Wojcech Swieszkowski, ClemensVan Blitterswijk & Lorenzo Moroni. Gradients in pore size enhance the osteogenic differentiation of human mesenchymal stromal cells in three-dimensional scaffolds. *Scientific reports* **2015**.

(114) Du, Y.; Liu, H.; Yang, Q.; Wang, S.; Wang, J.; Ma, J.; Noh, I.; Mikos, A. G.; Zhang, S. Selective laser sintering scaffold with hierarchical architecture and gradient composition for osteochondral repair in rabbits. *Biomaterials* **2017**, *137*, 37-48.

(115) Melchels, F. P.; Tonnarelli, B.; Olivares, A. L.; Martin, I.; Lacroix, D.; Feijen, J.; Wendt, D. J.; Grijpma, D. W. The influence of the scaffold design on the distribution of adhering cells after perfusion cell seeding. *Biomaterials* **2011**, *32*, 2878-2884.

(116) Phillippi, J. A.; Miller, E.; Weiss, L.; Huard, J.; Waggoner, A.; Campbell, P. Microenvironments engineered by inkjet bioprinting spatially direct adult stem cells toward muscle-and bone-like subpopulations. *Stem cells* **2008**, *26*, 127-134.

(117) Woodfield, T.; Blitterswijk, C. V.; Wijn, J. D.; Sims, T.; Hollander, A.; Riesle, J. Polymer scaffolds fabricated with pore-size gradients as a model for studying the zonal organization within tissue-engineered cartilage constructs. *Tissue engineering* **2005**, *11*, 1297-1311.

(118) Klein, T. J.; Rizzi, S. C.; Reichert, J. C.; Georgi, N.; Malda, J.; Schuurman, W.; Crawford, R. W.; Hutmacher, D. W. Strategies for zonal cartilage repair using hydrogels. *Macromolecular bioscience* **2009**, *9*, 1049-1058.

(119) Tamaddon, M.; Wang, L.; Liu, Z.; Liu, C. Osteochondral tissue repair in osteoarthritic joints: clinical challenges and opportunities in tissue engineering. *Bio-design and manufacturing* **2018**, 1-14.

(120) Yeatts, A. B.; Fisher, J. P. Bone tissue engineering bioreactors: dynamic culture and the influence of shear stress. *Bone* **2011**, *48*, 171-181.

(121) He, J.; Guo, J.; Jiang, B.; Yao, R.; Wu, Y.; Wu, F. Directing the osteoblastic and chondrocytic differentiations of mesenchymal stem cells: matrix vs. induction media. *Regenerative biomaterials* **2017**, *4*, 269-279.

(122) McBride, S. H.; Falls, T.; Knothe Tate, M. L. Modulation of stem cell shape and fate B: mechanical modulation of cell shape and gene expression. *Tissue Engineering Part A* **2008**, *14*, 1573-1580.

(123) Kreke, M. R.; Huckle, W. R.; Goldstein, A. S. Fluid flow stimulates expression of osteopontin and bone sialoprotein by bone marrow stromal cells in a temporally dependent manner. *Bone* **2005**, *36*, 1047-1055.

(124) Lee, D. A.; Knight, M. M.; Campbell, J. J.; Bader, D. L. Stem cell mechanobiology. *Journal of cellular biochemistry* **2011**, *112*, 1-9.

(125) Kim, K. M.; Choi, Y. J.; Hwang, J.-H.; Kim, A. R.; Cho, H. J.; Hwang, E. S.; Park, J. Y.; Lee, S.-H.; Hong, J.-H. Shear stress induced by an interstitial level of slow flow increases the osteogenic differentiation of mesenchymal stem cells through TAZ activation. *PloS one* **2014**, *9*, e92427.

(126) Sumanasinghe, R. D.; Bernacki, S. H.; Loboa, E. G. Osteogenic differentiation of human mesenchymal stem cells in collagen matrices: effect of uniaxial cyclic tensile strain on bone morphogenetic protein (BMP-2) mRNA expression. *Tissue engineering* **2006**, *12*, 3459-3465.

(127) Michalopoulos, E.; Knight, R. L.; Korossis, S.; Kearney, J. N.; Fisher, J.; Ingham, E. Development of methods for studying the differentiation of human mesenchymal

stem cells under cyclic compressive strain. *Tissue Engineering Part C: Methods* **2011**, *18*, 252-262.

(128) Pelaez, D.; Arita, N.; Cheung, H. S. Extracellular signal-regulated kinase (ERK) dictates osteogenic and/or chondrogenic lineage commitment of mesenchymal stem cells under dynamic compression. *Biochemical and biophysical research communications* **2012**, *417*, 1286-1291.

(129) Pauwels, F.: Grundrib einer Biomechanik der Fraktrheilung. 34th Kongress der Deutschen Orthopadischen Gesellschaft Ferdinand Enke Verlag, Stuttgart (1980)(Biomechanics of the locomotor apparatus). P. Manquet and R. Furlong. Berlin, Spinger, 1941.

(130) Perren, S. Physical and biological aspects of fracture healing with special reference to internal fixation. *Clinical orthopaedics and related research* **1979**, *138*, 175-196.

(131) Carter, D.; Blenman, P.; Beaupre, G. Correlations between mechanical stress history and tissue differentiation in initial fracture healing. *Journal of Orthopaedic Research* **1988**, *6*, 736-748.

(132) Carter, D. R.; Wong, M.; Orr, T. E. Musculoskeletal ontogeny, phylogeny, and functional adaptation. *Journal of Biomechanics* **1991**, *24*, 3-16.

(133) Claes, L. E.; Heigele, C. A.; Neidlinger-Wilke, C.; Kaspar, D.; Seidl, W.; Margevicius, K. J.; Augat, P. Effects of mechanical factors on the fracture healing process. *Clinical orthopaedics and related research* **1998**, *355*, S132-S147.

(134) Prendergast, P.; Huiskes, R.; Søballe, K. Biophysical stimuli on cells during tissue differentiation at implant interfaces. *Journal of biomechanics* **1997**, *30*, 539-548.

(135) Huiskes, R.; Van Driel, W.; Prendergast, P.; Søballe, K. A biomechanical regulatory model for periprosthetic fibrous-tissue differentiation. *Journal of materials science: Materials in medicine* **1997**, *8*, 785-788.

(136) Liu, X.; Niebur, G. L. Bone ingrowth into a porous coated implant predicted by a mechano-regulatory tissue differentiation algorithm. *Biomechanics and Modeling in Mechanobiology* **2008**, *7*, 335.

(137) Geris, L.; Andreykiv, A.; Van Oosterwyck, H.; Vander Sloten, J.; Van Keulen, F.; Duyck, J.; Naert, I. Numerical simulation of tissue differentiation around loaded titanium implants in a bone chamber. *Journal of biomechanics* **2004**, *37*, 763-769.

(138) Byrne, D. P.; Lacroix, D.; Planell, J. A.; Kelly, D. J.; Prendergast, P. J. Simulation of tissue differentiation in a scaffold as a function of porosity, Young's modulus and dissolution rate: application of mechanobiological models in tissue engineering. *Biomaterials* **2007**, *28*, 5544-5554.

(139) Melchels, F. P.; Bertoldi, K.; Gabbrielli, R.; Velders, A. H.; Feijen, J.; Grijpma, D. W. Mathematically defined tissue engineering scaffold architectures prepared by stereolithography. *Biomaterials* **2010**, *31*, 6909-6916.

(140) Gleadall, A.; Visscher, D.; Yang, J.; Thomas, D.; Segal, J. Review of additive manufactured tissue engineering scaffolds: relationship between geometry and performance. *Burns & trauma* **2018**, *6*, 19.

(141) Schipani, R.; Nolan, D. R.; Lally, C.; Kelly, D. J. Integrating finite element modelling and 3D printing to engineer biomimetic polymeric scaffolds for tissue engineering. *Connective Tissue Research* **2020**, *61*, 174-189.

(142) Olivares, A. L.; Marsal, È.; Planell, J. A.; Lacroix, D. Finite element study of scaffold architecture design and culture conditions for tissue engineering. *Biomaterials* **2009**, *30*, 6142-6149.

(143) Grayson, W. L.; Fröhlich, M.; Yeager, K.; Bhumiratana, S.; Chan, M. E.; Cannizzaro, C.; Wan, L. Q.; Liu, X. S.; Guo, X. E.; Vunjak-Novakovic, G. Engineering

anatomically shaped human bone grafts. *Proceedings of the National Academy of Sciences* **2010**, *107*, 3299-3304.

(144) Verhaegen, J.; Clockaerts, S.; Van Osch, G.; Somville, J.; Verdonk, P.; Mertens, P. TruFit plug for repair of osteochondral defects—where is the evidence? Systematic review of literature. *Cartilage* **2015**, *6*, 12-19.

(145) Longley, R.; Ferreira, A. M.; Gentile, P. Recent approaches to the manufacturing of biomimetic multi-phasic scaffolds for osteochondral regeneration. *International journal of molecular sciences* **2018**, *19*, 1755.

(146) Dell'Osso, G.; Bottai, V.; Bugelli, G.; Manisco, T.; Cazzella, N.; Celli, F.; Guido, G.; Giannotti, S. The biphasic bioresorbable scaffold (Trufit®) in the osteochondral knee lesions: long-term clinical and MRI assessment in 30 patients. *Musculoskeletal surgery* **2016**, *100*, 93-96.

(147) Kon, E.; Filardo, G.; Perdisa, F.; Di Martino, A.; Busacca, M.; Balboni, F.; Sessa, A.; Marcacci, M. A one-step treatment for chondral and osteochondral knee defects: clinical results of a biomimetic scaffold implantation at 2 years of follow-up. *Journal of Materials Science: Materials in Medicine* **2014**, *25*, 2437-2444.

(148) Kon, E.; Filardo, G.; Di Martino, A.; Busacca, M.; Moio, A.; Perdisa, F.; Marcacci, M. Clinical results and MRI evolution of a nano-composite multilayered biomaterial for osteochondral regeneration at 5 years. *The American journal of sports medicine* **2014**, *42*, 158-165.

(149) Christensen, B. B.; Foldager, C. B.; Jensen, J.; Jensen, N. C.; Lind, M. Poor osteochondral repair by a biomimetic collagen scaffold: 1-to 3-year clinical and radiological follow-up. *Knee surgery, sports traumatology, arthroscopy* **2016**, *24*, 2380-2387.

(150) Li, X.; Ding, J.; Wang, J.; Zhuang, X.; Chen, X. Biomimetic biphasic scaffolds for osteochondral defect repair. *Regenerative biomaterials* **2015**, *2*, 221-228.

(151) Wang, C.; Feng, N.; Chang, F.; Wang, J.; Yuan, B.; Cheng, Y.; Liu, H.; Yu, J.; Zou, J.; Ding, J. Injectable Cholesterol - Enhanced Stereocomplex Polylactide Thermogel Loading Chondrocytes for Optimized Cartilage Regeneration. *Advanced healthcare materials* **2019**, *8*, 1900312.